University of Groningen

The effects of social environment on AD-related pathology in hAPP-J20 mice and tau-P301L mice

Lanooij, Suzanne D; Drinkenburg, W H I M; Eisel, U L M; van der Zee, E A; Kas, Martien J H

IMPORTANT NOTE: You are advised to consult the publisher's version (publisher's PDF) if you wish to cite from it. Please check the document version below.

Document Version
Publisher's PDF, also known as Version of record

Publication date:
2023

[Link to publication in University of Groningen/UMCG research database](#)
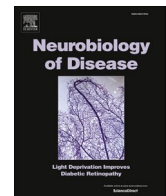
The effects of social environment on AD-related pathology in hAPP-J20 mice and tau-P301L mice

Suzanne D. Lanooij [a], W.H.I.M. Drinkenburg [a,b], U.L.M. Eisel [a], E.A. van der Zee [a], Martien J. H. Kas [a,*]

[a] Groningen Institute for Evolutionary Life Sciences (GELIFES), Neurobiology, University of Groningen, Nijenborgh 7, 9747, AG, Groningen, the Netherlands
[b] Department of Neuroscience, Janssen Research & Development, a Division on Janssen Pharmaceutica NV, Turnhoutseweg 30, B-2340 Beerse, Belgium

ARTICLE INFO

ABSTRACT

In humans, social factors (e.g., loneliness) have been linked to the risk of developing Alzheimer's Disease (AD). To date, AD pathology is primarily characterized by amyloid-β plaques and tau tangles. We aimed to assess the effect of single- and group-housing on AD-related pathology in a mouse model for amyloid pathology (J20, and WT controls) and a mouse model for tau pathology (P301L) with and without seeding of synthetic human tau fragments (K18).

Female mice were either single housed (SH) or group housed (GH) from the age of 6–7 weeks onwards. In 12-week-old P301L mice, tau pathology was induced through seeding by injecting K18 into the dorsal hippocampus (P301L$_{K18}$), while control mice received a PBS injection (P301L$_{PBS}$). P301L mice were sacrificed at 4 months of age and J20 mice at 10 months of age. In all mice brain pathology was histologically assessed by examining microglia, the CA1 pyramidal cell layer and specific AD pathology: analysis of plaques in J20 mice and tau hyperphosphorylation in P301L mice.

Contrary to our expectation, SH-J20 mice interestingly displayed fewer plaques in the hippocampus compared to GH-J20 mice. However, housing did not affect tau hyperphosphorylation at Ser202/Thr205 of P301L mice, nor neuronal cell death in the CA1 region in any of the mice. The number of microglia was increased by the J20 genotype, and their activation (based on cell body to cell size ratio) in the CA1 was affected by genotype and housing condition (interaction effect). Single housing of P301L mice was linked to the development of stereo-typic behavior (i.e. somersaulting and circling behavior). In P301L$_{K18}$ mice, an increased number of microglia were observed, among which were rod microglia.

Taken together, our findings point to a significant effect of social housing conditions on amyloid plaques and microglia in J20 mice and on the development of stereotypic behavior in P301L mice, indicating that the social environment can modulate AD-related pathology.

1. Introduction

Dementia is an umbrella term for neurodegenerative disorders associated with devastating progressive cognitive decline and is estimated to affect over 55 million people worldwide. In addition, it constitutes a major health concern that results in a high social and economic burden and calls for effective therapies. Alzheimer's Disease (AD), which is responsible for 60–70% of the dementia cases, is a multifactorial syndrome with age being the major risk factor. In AD, it is now well established that several lifestyle factors (e.g., diet, physical activity,

education) are linked to the risk and course of AD (Lenart-Bugla et al., 2022). Modifiable lifestyle factors can be seen as potential targets for therapies, as they may be more cost-effective and have less side effects compared to pharmacotherapy (McRae et al., 2021; Walsh et al., 2022). Over the past years, accumulating evidence has linked social factors to the development of AD (Evans et al., 2018; Fleck et al., 2019; Penninkilampi et al., 2018; Piirainen et al., 2017; Shen et al., 2022). People with a strong social network have been found to have a lower risk of developing dementia and a slower rate of cognitive decline compared to those who are socially isolated and/or experience loneliness (Evans

---

et al., 2018; Fleck et al., 2019; Penninkilampi et al., 2018; Piirainen et al., 2017; Shen et al., 2022). Therefore, this study examines the relationship between the social environment and AD-related pathology.

Neuropathologically, AD is characterized by the presence of amyloid-β (Aβ) plaques and neurofibrillary tau tangles (NFTs) in the brain, eventually resulting in severe atrophy (Braak and Braak, 1991). The medial temporal lobe is the earliest region to be affected, followed by other cortical and subcortical areas. The hippocampus has been a primary region of study in the context of AD, because of its vital role in learning and memory and its vulnerability to AD-pathology (Lakshmisha Rao et al., 2022). Especially the CA1 region is highly vulnerable to AD pathology, exhibiting synaptic loss and atrophy (Lakshmisha Rao et al., 2022; Wright et al., 2013). Importantly, the pathological conditions that underlie AD commence years to decades before the clinical diagnosis, suggesting that aiming to prevent or delay pathology may be a more effective treatment approach than aiming to cure AD clinical symptoms.

Amyloid-β plaques are mainly composed of Aβ peptides derived from proteolytic cleavage of the amyloid precursor protein (APP). An increased production and/or reduced clearance of these fibrils leads to extracellular plaque deposition. In contrast to the original amyloid hypothesis, not the amyloid-β plaques but the soluble oligomeric Aβ fragments are most neurotoxic (Mucke and Selkoe, 2012). In addition, NFTs are composed of hyperphosphorylated tau protein aggregates. Tau constitutes an important microtubule-associated protein, and its activity is tightly regulated by phosphorylation. Hyperphosphorylation of the tau protein at specific sites (e.g., Ser202/Thr205) leads to loss of normal function or gain of toxic function, resulting in misfolding of the protein which distorts normal functioning of the cell (Wang and Mandelkow, 2016). Misfolded tau aggregates eventually result in the formation of intraneuronal NFTs. It is suggested that misfolded tau proteins can spread from one neuron to another in a prion-like manner, inducing tau pathology and thereby synaptic dysfunction in those cells (Mudher et al., 2017; Wang and Mandelkow, 2016). According to the amyloid cascade hypothesis, the pathological cascade of AD is initiated by amyloid pathology with tau pathology being a downstream effect of this cascade. Moreover, these two core pathological hallmarks do not act independently but synergistically (Bloom, 2014; Busche and Hyman, 2020; Roda et al., 2022).

In this paper we will use two prominent transgenic mouse models that are built on the above insights: the J20 mouse model and the P301L mouse model. The J20 mouse model expresses human Amyloid Precursor Protein (hAPP) with the Indiana and Swedish mutation under the PDGF promoter, resulting in overexpression of hAPP and increased Aβ formation. As a consequence, these mice display cognitive deficits and plaque formation from approximately 5 months of age. The P301L mice express the longest human isoform of the tau protein, with the P301L mutation. The P301L mutation has been linked to frontotemporal dementia, and is a commonly used mutation for the study of tau pathology in AD mouse models. The tau P301L transgenic mice in this study will be used as a tau seeding model, which allows controlled onset of tau pathology. Tau seeding is obtained by injecting tau fibrils containing the P301L mutation (K18) into the hippocampus, which results in rapid spread of tau hyperphosphorylation in these transgenic P301L mice (P301L$_{K18}$ mice) (Peeraer et al., 2015).

Another key player in the pathogenesis of AD is neuroinflammation. Microglial cells are the resident immune cells of the brain and provide immune surveillance. In addition, microglia can remove pathogens and debris and contribute to the maintenance of synaptic homeostasis. They become activated by pathological triggers, like neuronal death or protein aggregates, leading to migration of the cells to the lesion and activation of the innate immune response (Leng and Edison, 2021). This initial acute inflammatory response aids to restore tissue homeostasis, however, sustained activation leads to chronic inflammation which causes synaptic dysfunction and neuronal death.

The exact role of microglia in AD disease progression is to be elucidated (ElAli and Rivest, 2016; Odfalk et al., 2022). Microglia are involved in the clearance of Aβ, especially in the early stages of the disease. In addition, they have been demonstrated to be able to internalize and degrade tau protein (ElAli and Rivest, 2016; Odfalk et al., 2022). In contrast, microglia activated by Aβ release pro-inflammatory cytokines and neurotoxic molecules, contributing to a neurodegenerative cascade. Furthermore, activated microglia have been shown to be able to initiate tau pathology (ElAli and Rivest, 2016; Odfalk et al., 2022). Correspondingly, microglia activation correlates with both amyloid deposition and tau aggregations in AD patients (Dani et al., 2018). This association is also observed in AD mouse models. For example, adult J20 mice have been shown to display a higher number and coverage of hippocampal microglia compared to WT mice (Ameen-Ali et al., 2019; Wright et al., 2013). Furthermore, microglia activity and number are closely linked to tau hyperphosphorylation in the presence of the tau P301L mutation (Jaworski et al., 2011; Peeraer et al., 2015; Sasaki et al., 2008).

Animal studies can provide insight into the causal relationship between social factors and dementia pathophysiology. Indeed, mouse studies have shown negative effects of single housing (social isolation) on cognitive tasks (Bianchi et al., 2006; Templer et al., 2019; Wang et al., 2020), but the effect of social isolation on AD pathophysiology requires further investigation. A few studies have found an increase in dementia-related pathology (e.g., the number of plaques, alteration in neuroinflammatory state) and decreased cognitive functioning upon social isolation of AD-transgenic mice (Dong et al., 2004; Huang et al., 2015; Liang et al., 2019; Peterman et al., 2020). Yet, an effect of social interventions on plaques is not consistently observed (Liang et al., 2019; Pietropaolo et al., 2009) and several methodological differences exist (Table 1).

While the majority of these studies focused on APP-pathology, there remains a paucity for the effect of social isolation in tau-transgenic mice. In addition, the vast majority of preclinical studies into AD used male mice only, while AD is more prevalent in females. Moreover, female mice have been shown to be more vulnerable to the detrimental effects of restraint and environmental stress (including social stress (van Doeselaar et al., 2021)), and this has been linked to increased Aβ and tau pathology in females but not in males (Devi et al., 2010; Sotiropoulos et al., 2015). Therefore, in the current study, we aimed to examine the effect of the social environment (single housing or group housing) on two core pathological events of AD pathophysiology using two different female mouse models: J20 mice to study APP-pathology and P301L mice with tau seeding to study tau propagation.

For both mouse models, the single housing was started during the adolescence age, as studies have repeatedly shown that this age constitutes a critical period for detrimental effects caused by social experiences, including social isolation (Hall, 1998; Lander et al., 2017; Medendorp et al., 2018; Riviera-Irizarry et al., 2020). The effect of the social environment on AD-related pathology was histologically investigated by examining the core pathological hallmarks (Aβ plaques in J20 mice, tau hyperphosphorylation in P301L mice), microglia, and the thickness of the CA1 pyramidal cell layer. The time-point for histological examination was chosen to ensure the presence of sufficient plaques (10 months in J20 mice) or hyperphosphorylated tau (one-month post-seeding in P301L mice) in order to see an effect of the social housing condition on these readouts. We hypothesized that single housed mice would display deteriorated brain health as evident from increased AD-related pathology. We found a minor effect of the social environment on brain health, but surprisingly, in contrary to our hypothesis, we observed decreased plaque load in single housed J20 mice compared to group housed J20 mice. Both the J20 mice and the P301L$_{K18}$ mice showed increased microglia number and activation and signs of neurodegeneration of the CA1 pyramidal cell layer compared to control mice.

3

Table 1

Literature overview on social manipulations in AD mice. SH = single housed, GH = group housed. Only the results relevant to our study (i.e. markers that we also measured) of the experimental groups without interventions besides the social housing were included in this table.

	Huang et al. (2015)	Liang et al. (2019)	Peterman et al. (2020)	Pietropaolo et al. (2009)	Hsiao et al. (2011)	Dong et al. (2004)	Our study
Mouse model	APP/PS-1	APP/PS-1	5x FAD	3× Tg-AD	APP/PS-1	Tg2576	J20 P301L
Gender	Males	Males	Males	Males and females	Males	Males and females	Females
Cage size (L x W x H)	not reported	not reported	GH: 30 × 25 × 30 cm	GH: 41 × 20 × 19 cm, SH: 26 × 21 × 14 cm	not reported	GH:27 × 14 × 9.5 cm SH: 10 × 14 × 9.5 cm	32 × 16 × 14 cm
Mice per cage (group housed)	4 mice	6 mice	3–4 mice	4–5 mice (same-sex)	4 mice	3 mice	4 mice
Floor space per mouse	not reported	not reported	GH: 188–250 cm^2/mouse	GH: 164–205 cm^2/mouse	not reported	GH: 126 cm^2/mouse SH: 140 cm2/mouse	GH: 128 cm^2/mouse SH: 512 cm2/mouse
Cage enrichment and cleaning	not reported	not reported	not reported	sawdust bedding, weekly cage cleaning, wired lids	not reported	not reported	paper roll, nesting material, red Igloo (P301L mice only), weekly cleaning
Holding room characteristics	not reported	not reported	not reported	22 °C, 55% humidity	not reported	SH and GH mice located in seperate rooms	All cages in the same holding room, 21 °C, 55% humidity
Age at start intervention	17 months	6 months	2 months	21 days (post-weaning)	1 month	post-weaning	6–7 weeks
Intervention duration	3 months	6 months	2 or 3 months	5.5 months	8 weeks	5 months	8.5 months (J20) 10 weeks (P301L)
Age at examination	20 months	12 months	4–5 months	180 days	3 months	6 months	10 months (J20) 16 weeks (P301L)
Relevant results	• SH mice displayed increased hippocampal plaque coverage compared to GH mice • SH mice increased GFAP and IBA-1 immunoreactivity	• Plaque load remained unaffected by the social housing condition Compared to GH mice, SH mice and mice housed with one female had: • more pro-inflammatory mediators and less anti-inflammatory mediators on hippocampal microglia • less GFAP immunoreactivity	• SH mice displayed increased number of hippocampal plaques compared to GH mice	• Females displayed more severe Aβ pathology in the hippocampus compared to males. • No effect of the social housing condition on Aβ pathology	• SH mice had higher Aβ concentration (hippocampal lysate) compared to GH mice	• SH Tg mice had more Aβ plaques compared to GH Tg mice	• GH J20 mice more plaques compared to SH mice • More stereotypic behavior in SH-P301L mice compared to GH-P301L mice

2. Materials and method

2.1. Animals

J20 mice: J20 mice (Mucke et al., 2000) were obtained through in-house breeding by crossing heterozygous animals with WT (C57BL/6) animals. J20 mice were heterozygous with respect to the transgene, which was verified by PCR on ear clip material (internal control forward primer oIMR8744 5'-CAAATGTTGCTTGTCTGGTG, internal control reverse primer oIMR8745 5'- GTCAGTCGAGTGCACAGTTT, transgene forward primer oIMR2044 5'-GGTGAGTTTGTAAGTGATGCC, oIMR2045 transgene reverse primer 5'-TCTTCTTCTTCCACCTCAGC). The genotype was reconfirmed from new ear clip material after termination of the animal at the end of the experiment. Non-transgenic littermates were used as controls and are referred to as WT mice. Only female mice were used for this study. Littermates were randomly distributed over different cages and all mice were housed in groups of four mice with the same genotype. Based on a power calculation based on literature, a total of 57 mice (obtained over three breeding batches) were bred for this study. As sudden early death is common among J20 mice, extra mice were included in this study. In total, ten J20 mice suffered from early death during the experimental period (3 isolated J20 mice, 7 group housed J20 mice). Two WT mice were excluded because of welfare issues; one mouse had hydrocephalus and the other mouse displayed signs of discomfort that reached the humane endpoint. As a result, 45 mice were used for histochemical purposes (GH-WT mice, *n* = 11; SH-WT mice, *n* = 12; GH-J20 mice, *n* = 10; SH-J20 mice, n = 12). Mice were sacrificed when they were 10 months old (Fig. 1).

P301L mice: Female transgenic tauP301L mice (FVB/N) expressing the longest human tau isoform with the P301L mutation (tau-4R/2 N-P301L) under control of the *thy1* gene promotor (homozygous) (Terwel et al., 2005) were provided by Janssen Pharmaceutica NV (bred at Janssen Pharmaceutica, Beerse, Belgium). The transgene results in the development of tau pathology by the age of 9 months (Terwel et al., 2005). Upon arrival, the litters were distributed over cages in groups of

four. Mice were delivered in eight batches, and divided into three different study cohorts: cohort 1 (containing mice from batch 1 and 2, *n* = 15), cohort 2 (containing mice from batch 3–8, *n* = 88), cohort 3 (containing mice from batch 1–4, *n* = 40). Cohort 1 was used to assess the effect of the social environment on microglia activity (e.g., number and morphology) in 12-week-old mice that did not receive a hippocampal injection. Cohort 2 and 3 received a hippocampal injection at 12 weeks of age and were sacrificed one month later (Fig. 1). Additionally, mice of cohort 2 underwent behavioral experiments (Appendix II of this thesis). One mouse of cohort 2 died during the stereotaxic surgery and one mouse was excluded from the experiment as it was severely attacked by its cage mates the day after redistributing the mice over cages. All histological analyses were performed on cohort 2, unless specified otherwise. Two brain samples of cohort 2 could not be used for immunohistochemistry due to severe freezing artifacts, resulting in a total of 84 brains (*n* = 19–24 per group). The brain samples of cohort 3 were histologically assessed by Janssen Pharmaceutica (Beerse, Belgium).

2.2. Housing intervention

The social environment was manipulated by varying the housing condition of mice; single-housing (referred to as SH or social isolation) and group housing (referred to as GH). When mice were 6–7 weeks old, the cages were randomly assigned to continue group housing (4 mice per cage) or to undergo social isolation (see 'Animals' section for the number of animals per experimental group). Our social isolation protocol entailed individual housing of the mouse, with identical cage size, enrichment, cleaning frequency, and holding room to that of group housed mice. Mice that were assigned to be group housed remained housed in the same group composition, but received a clean cage, bedding, nesting material, paper roll, and red house at the day the mice from the social isolation group were housed individually. All mice were housed in the same holding room.

All mice were housed in type II-L Makrolon cages (32 × 16 × 14 cm) with wired lids (without filter tops), with bedding (Aspen), and enriched
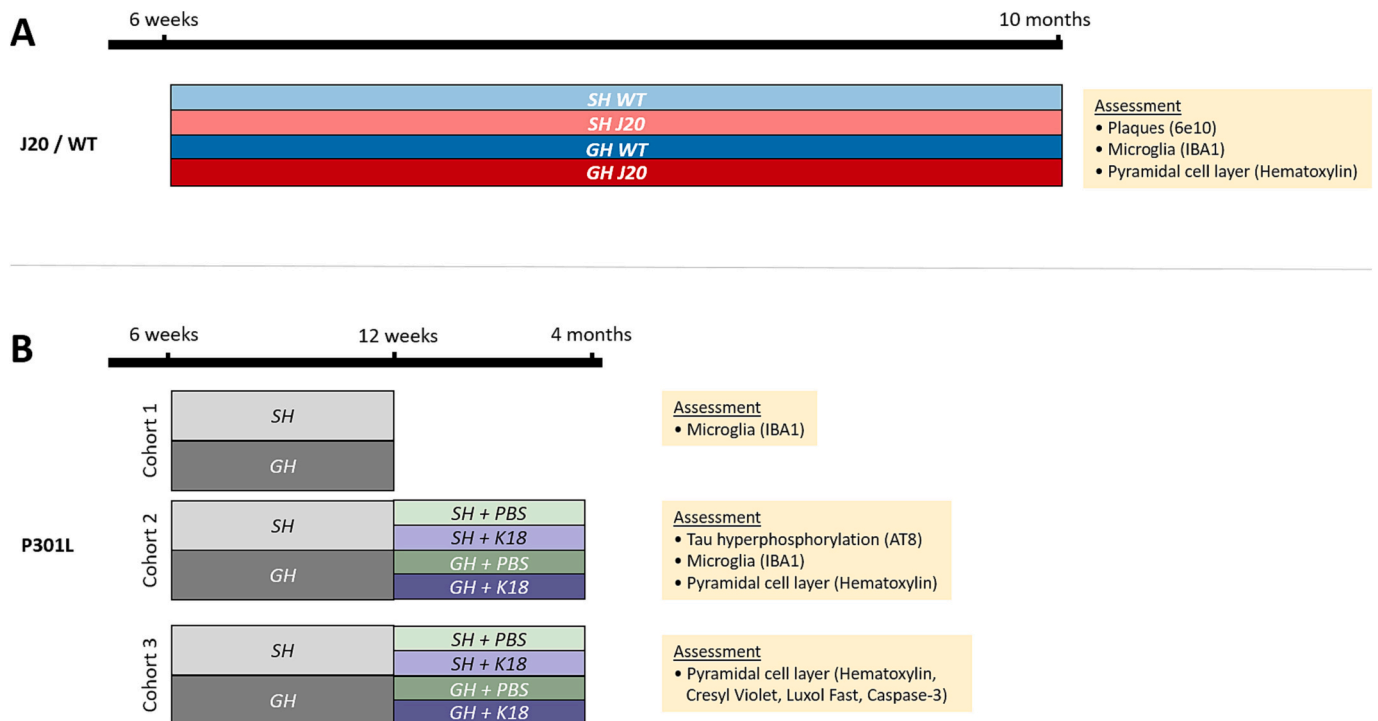
Fig. 1. *Study design.* The social environmental manipulation (social isolation; SH) was started when mice were 6–7 weeks old. Half of the mice remained group housed (GH). A) J20 and WT littermates were sacrificed at 10 months of age. B) P301L mice of cohort 2 and 3 were injected with PBS or K18 into the hippocampus at 12 weeks of age.

with nesting material (Envirodry), and a paper roll. P301L mice also had a red mouse Igloo (10.8 cm wide x 5.7 cm tall, with 3 openings) in their cage, as this may slow down their retinal degeneration. Food (chow, Altromin) and tap water were available ad libitum. Mice were housed under standard 12:12 light/dark conditions (lights off at 13.00 h) at 21 $\pm$ 1° degrees and humidity 45–65%. Cages were cleaned every week. All experimental procedures were approved by the Ethical Committee of the University of Groningen and complied with the principles of good laboratory animal care following the European Directive 2010/63/EU for animal experiments. In addition, we applied the ARRIVE guidelines for reporting on animal research.

2.3. Tau seeding

Synthetic human tau fragments (K18) were prepared according to a previously established method (Peeraer et al., 2014) and provided by Janssen Pharmaceutica NV, Belgium. These fragments consisted of human tau fragments containing the P301L mutation in phosphate buffered saline (PBS). Sonication of K18 was done <5 days before the hippocampal injection to create tau fibrils and potentiate prion seeding, using a short protocol of 2 min (amplitude 15%, 2 s pulses with 10 s interval, using the Branson SFX 250). Samples were kept on ice during the sonification procedure. Sonicated K18 samples were stored at −80 °C until used for the seeding injections.

The protocol for the hippocampal injection was adopted from Peeraer et al. (Peeraer et al., 2014). P301L mice of 12 weeks of age were deeply anesthetized by isoflurane for stereotaxic surgery. The head was shaved, and the skin was cleaned with Betadine. After fixating the head with cheek bars in the stereotactic apparatus, eye cream was applied and a Carpofen injection (0.1 mL/10 g) was given (intraperitoneal) as general analgesia. After the incision was made, a local anesthetic (Lidocaine) was applied. Sonicated K18 or vehicle (PBS) was injected unilaterally into the right dorsal hippocampus (A/P -2.5 mm; L + 2.0 mm; D/V -2.4 mm). A tilt factor (calculated by dividing the distance between Bregma and Lambda in mm by 0.421) was multiplied with the A/P coordinate of the injection site to adjust the relative A/P coordinate to the size of the brain. A volume of 2 μL was injected with a speed of 2 μL/min. After the injection, the needle was kept in place for an additional 3 min before gentle withdrawal. Half of the P301L cages of each housing condition were injected with synthetic tau fibrils and the other half with vehicle; 20 GH-P301L $_{PBS}$ mice, 19 SH-P301L $_{PBS}$ mice, 24 GH-P301L $_{K18}$ mice, and 21 SH-P301L$_{K18}$ mice. Conditions were assigned randomly, mice housed in the same cage always received the same hippocampal injection. Group housed mice were individually housed after their surgery and placed back together an hour after the last mouse from that group had woken up from the surgical procedure.

2.4. Tissue collection and processing

J20 and WT mice were sacrificed by perfusion at the age of 10 months. P301L mice were sacrificed by perfusion at the age of 4 months, one month after the tau-seeding. The procedure was the same for both mouse lines. Mice were anesthetized with 0.1 mL Pentobarbital. Transcardial perfusion was done with 150 mL 0.9% NaCl + Heparin solution, followed by 150 mL of 4% PFA. Mice were decapitated and the brain was taken out and post-fixated in 4% PFA for 18–24 h at room temperature (RT). After post-fixation, brains were washed three times with 0.01 M PB. Eventually, brains were put through a sucrose gradient (10% for 1 h, 20% for ±5 h, 30% overnight) for cryopreservation. When the brains had sunk to the bottom of the tissue cup, the brains were snap-frozen using liquid nitrogen and stored in a − 80 freezer upon cryosectioning. Brains of the P301L mice were marked with a small incision on the left (contralateral) cortex, to be able to distinguish between the ipsilateral and contralateral hemisphere after sectioning. Coronal brain sections of 20 μm were cut using a Leica CM3050 or Leica CM1860 and stored in PBS with 1% sodium azide at 4 °C until used for histology.

2.5. Immunohistochemistry

Immunohistochemical DAB (3,3'-Diaminobenzidine) stainings were performed on tissue sections in order to visualize amyloid plaques, tau hyperphosphorylation at Ser202/Thr205, and microglia. Sections were washed with 0.1 M PBS or 0.1 M TBS buffer, depending on the antibody used. Negative control samples consisted of tissue sections of two mice (randomly selected) of which positive staining was expected, and underwent the same staining procedure except that they were not incubated with the primary antibody. All washing and incubation steps were done on a shaker at room temperature, unless specified otherwise.

2.5.1. 6e10

Amyloid-β plaques in the J20 mouse line were visualized using a 6e10 antibody. Four sections per animal containing the dorsal hippocampus (between Bregma −1.55 and − 2.35) were selected for the staining. Sections were washed 3× with 0.01 M TBS buffer for 5 min and blocked with 0.3% H_2O_2 in TBS for 30 min. After washing, sections were pre-incubated with 0.1% Triton X-100 and 3% goat serum for 1 h. Then, sections were incubated with the primary antibody 6e10 (1:1000, Biolegend 803,003) in TBS containing 0.1% Triton X-100 and 3% goat serum for 3 nights at 4 °C. After washing away the primary antibody, sections were incubated with 1:400 biotin conjugated secondary antibody goat-anti-mouse in TBS containing 1% goat serum for 2 h. After extensive washing, sections were incubated for 1.5 h with 1:500 avidin-biotin complexes (Vectastain ABC kit, Vector Laboratories) in TBS.

2.5.2. AT8

The AT8 antibody binds to hyperphosphorylated tau at Ser202/Thr205, one of the critical phosphorylation sites. This staining was performed on samples from cohort 2. For each animal, coronal sections of multiple locations were stained; 2 frontal slices (Bregma 2.4 until 2.8), 2 striatal slice (Bregma 0.3 until 1.0), 3 dorsal hippocampus slices (Bregma −2.1 until −1.5) and 2 ventral hippocampal slices (Bregma −3.0 until −2.5). Sections were washed 3× with 0.01 M TBS (Tris-base Buffered Saline) buffer for 5 min and blocked with 0.3% H_2O_2 in 0.01 M TBS for 30 min. After washing, sections were incubated with 1:1000 mouse anti-AT8 (MN1020, ThermoScientific) in TBS containing 1% BSA and 0.5% Triton X-100 for 2 h on room temperature, followed by 3 nights of incubation at 4 °C. After washing away the primary antibody solution, the sections were incubated with the biotin conjugated secondary goat-anti-mouse antibody (1:500, Jackson) in TBS for 2 h. After extensive washing, sections were incubated for 2 h with 1:500 avidin-biotin complexes (Vectastain ABC kit, Vector Laboratories) in TBS.

2.5.3. Ionized calcium binding adaptor molecule 1 (IBA1)

This staining was performed on brain samples of J20 mice and of P301L mice from cohort 1 and 2. Dorsal hippocampal sections were washed 3× with 0.01 M PBS (Phosphate Buffered Saline) for 5 min and blocked with 0.3% H_2O_2 in PBS for 30 min. After washing, sections were incubated with rabbit anti-IBA1 (1:2500, Wako Chemicals 019–19,741) in PBS containing 1% BSA and 0.1% Triton X-100 for 3 nights on a shaker at 4 °C. After washing, the samples were incubated with biotin conjugated secondary Goat-anti-Rabbit antibody (1:500) for 2 h. After extensive washing, sections were incubated for 1 h with 1:500 avidin-biotin complexes (Vectastain ABC kit, Vector Laboratories) in PBS.

Subsequently, sections were washed with a buffer before continuing with the DAB step. DAB solution was prepared by dissolving DAB tablets in MQ. The reaction was activated by adding 0.1% H_2O_2 to each sample and stopped by washing with the buffer solution. Sections were mounted on glass slides (Thermo Scientific) using gelatin and air dried overnight. After drying, sections were dehydrated in a series of Ethanol followed by Xylol and covered with DPX and a coverslip.

2.6. Hematoxylin staining

Dorsal hippocampal sections (between Bregma −1.55 and − 2.35) were mounted on poly-L-lysine coated slides (Thermo Fisher) and dried overnight. Sections were rinsed in MQ for 2 min, after which they were placed in Mayer's Hematoxylin (Merck HX314794) for 4 min. Hematoxylin was then washed away by placing the samples under lukewarm running tap water for 12 min. Slides were then rinsed in MQ for 1 min, and then dehydrated through 1 min in 95% EtOH, two times 5 min in 100% EtOH, followed by two times in 100% Xylene. Samples were covered with DPX and a coverslip.

2.7. Microscopy and image analysis

2.7.1. 6e10
Pictures were taken with a Leica DMI6000 B microscope (Leica microsystems) at $50\times$ magnification using the LAS-X Navigator software (Leica microsystems). Stitched images of the hippocampus were created using the Leica Navigator software.

The 6e10 staining was quantified by measuring coverage and optical density of the staining of the whole left and right hippocampus. For the coverage, the percentage of positively stained area was measured. A fixed threshold was used, which was determined after manual inspection of several images. To measure the optical density of the plaques, a Rodbard calibration was performed before measuring the intensity (ImageJ.nig.gov, n.d.). On the same sections, the plaque coverage was measured in the cortical area above the hippocampus, spanning from +3–4 mm to - 3-4 mm relative to the A/P midline (depending on the Bregma coordinate).

2.7.2. AT8
The AT8-immunoreactivity was assessed manually using a light microscope, by a researcher blinded for the housing conditions. A scoring system was made based on the intensity and amount of AT8 positive staining per region, ranging from 0 (no immuno-positive staining) to 5 (very high immune-positive staining) (see Supplementary Fig. 1). Pictures for publication were taken with the Leica DMI6000 B microscope at $50\times$ magnification. For the frontal cortex and lateral septum, no distinction was made between the ipsilateral and the contralateral side for quantification.

2.7.3. IBA1
Pictures were taken with the Leica DMI6000 B microscope at $200\times$ magnification. Using ImageJ, a region of interest (ROI) was drawn at the CA1 and the DG (indicated in blue in Fig. 3A). The ROI of the CA1 included the oriens, pyramidal, and radiatum layer and was on average 0.6 mm^2. The ROI for the DG included the inner blade, hilus, and outer blade and was approximately 1.0 mm^2. The number of microglia cell bodies and their size was determined by applying an automatic threshold (Triangle) followed by a size threshold of >35 μm^2. The number of microglia was based on the number of detected cell bodies and is expressed as the number of microglial cells per 10^5 px (i.e., ~0,34 mm^2). Using the automatic default threshold, the total cell size and the coverage (the percentage of area positive for the IBA1-staining) was determined. The activation status of the microglia, based on the cell body to cell size ratio, was determined by dividing the cell body size by the total cell size (Hovens et al., 2014). For the J20 mice and the WT control mice, both left and right hemispheres were analyzed. For the P301L mice, only the ipsilateral hemisphere was analyzed.

2.7.4. Hematoxylin
To assess the thickness of the CA1 pyramidal layer, the sections were photographed with a Leica Olympus BH2 microscope (Leica microsystems) at $100\times$ magnification and analyzed using ImageJ. The hematoxylin staining provided a clear contrast between the pyramidal cell layer and the oriens and radiatum, allowing ImageJ to set an automated

threshold and calculate the surface area (including holes). A rectangular region of interest (200 μm width) was drawn at an approximate straight part of the pyramidal cell layer. The mean height of the pyramidal cell layer was then calculated on the threshold image by dividing the surface area by the width of the rectangle.

In addition, for the J20 and WT mice, it was estimated whether genotype and/or housing condition affected the number of cells in the pyramidal cell layer of the CA1. For this, the hematoxylin sections were photographed at $400\times$ magnification using the Leica DMI6000 B microscope. By applying a segmentation analysis using ImageJ (Watershed) on a threshold image (Default threshold), the number of cells in a region of 186 μm width was estimated. A minimum particle size threshold was applied of 85 μm^2.

2.8. Monitoring stereotypic behavior

The expression of stereotypic behavior (e.g., repetitive circling, bar mouthing, somersaulting) in P301L mice was checked by the same researcher at least once per week during the dark phase. Mice remained in their home cage and were left undisturbed while being monitored for several minutes. Mice that displayed evident repetitive circling, bar mouthing, or somersaulting during those minutes were marked as being 'stereotypic'.

2.9. Qualitative histological analysis P301L brains cohort 3

Cryopreserved brains of P301L mice from cohort 3 were re-embedded in paraffin. Formalin-fixed paraffin embedded brains were sectioned at 5 μm thickness, mounted on precharged Superfrost Plus slides using a microtome (Microm HM360).

2.9.1. Hematoxylin
For histopathological evaluation, sections were stained using the Ventana HE600 automated stainer (Roche).

2.9.2. Luxol fast blue and Cresyl Violet
After deparaffinization, sections were stained in Luxol fast blue solution overnight (56–60 °C). Sections were rinsed in 96% EtOH until excess staining was removed. After rinsing the slides in demi water, the sections were differentiated using lithiumcarbonate. Then, the sections were differentiated with 96% EtOH until a distinction could be made between grey and white matter, followed by a rinsing step in demi water. Next, sections were incubated in cresyl-violet solution for 6 min at 57 °C. Differentiation was performed in different steps using 96% EtOH. Sections were then dehydrated in 100% EtOH two times for 2 min, followed by two times 2 min Xylene.

2.9.3. Caspase-3
Sections were stained automatically using Ventana discovery-ultra autostainer (Roche diagnostics, Rotkreuz-Switzerland). In brief, epitope retrieval was performed using CC1 (EDTA buffer) at 95 °C for 32 min. Endogenous peroxidases were blocked with inhibitor CM for 8 min. Incubation with the primary antibody (1:200, anti-cleaved-caspase-3, Cell signaling, #9664) was done for 32 min at 37 °C. Then, sections were incubated with the secondary antibody anti-rabbit HQ for 20 min followed by incubation with anti HQ HRP for 20 min. The binding was visualized using DAB. A negative control was included using an isotype control (1:200 rabbit monoclonal, Abcam, Ab125938).

2.10. Data analysis

Data were analyzed with R Studio ("RStudio Team, RStudio: Integrated Development for R,", 2020). Data were checked for normality using the Shapiro-Wilk test. For normally distributed data, the homogeneity of variance was checked with Barlett's test for independent *t*-tests and the NCV test for linear models. For non-normally distributed

data, Levene's test was used to assess homogeneity of variance. Non-normally distributed data that could not be normalized by a mathematical data transformation was analyzed with the non-parametric test (Wilcoxon rank sum test or Kruskal-Wallis test when comparing two groups) or generalized linear modeling (when comparing four groups with two predictor variables).

Independent t-tests or Wilcoxon rank sum tests were performed to analyze the 6e10 staining. Readouts from the 6e10 staining were analyzed using independent t-tests (coverage hippocampus) or Wilcoxon rank sum test (OD hippocampus and coverage in the cortex). The Kruskall-Wallis test was used to assess the effect of the housing condition on AT8 immunoreactivity.

Two-way ANOVA, linear models (LM), or generalized linear models (GLM) were used to assess the effect of housing (i.e., SH or GH), animal background (i.e., J20 or WT, or P301$_{K18}$ or P301L$_{PBS}$), and their interaction on the IBA1 and hematoxylin staining. The LM and GLM were constructed with the housing condition (single- or group-housing) and animal intervention (genotype (WT or J20) for the J20 mouse line, and injection (PBS or K18) for the P301L mouse line) as factor and tested for an interaction using the lmerTest package in R (Kuznetsova et al., 2017). Post-hoc multiple comparisons were performed with Tukey correction for multiple testing when the model showed a statistically significant effect for one of the factors (housing condition or animal background).

The relationship between stereotypic behavior and the social housing condition and injection was analyzed using Cox proportional hazard regression.

Data were plotted in R with the ggplot2 package (Wickham, 2016). Whiskers of the boxplots reach 1.5 x IQR from the upper or bottom hinge of the box. Values outside of this range are indicated with a black dot. Statistical outliers (IQR method) were removed if this interfered with the statistical model.
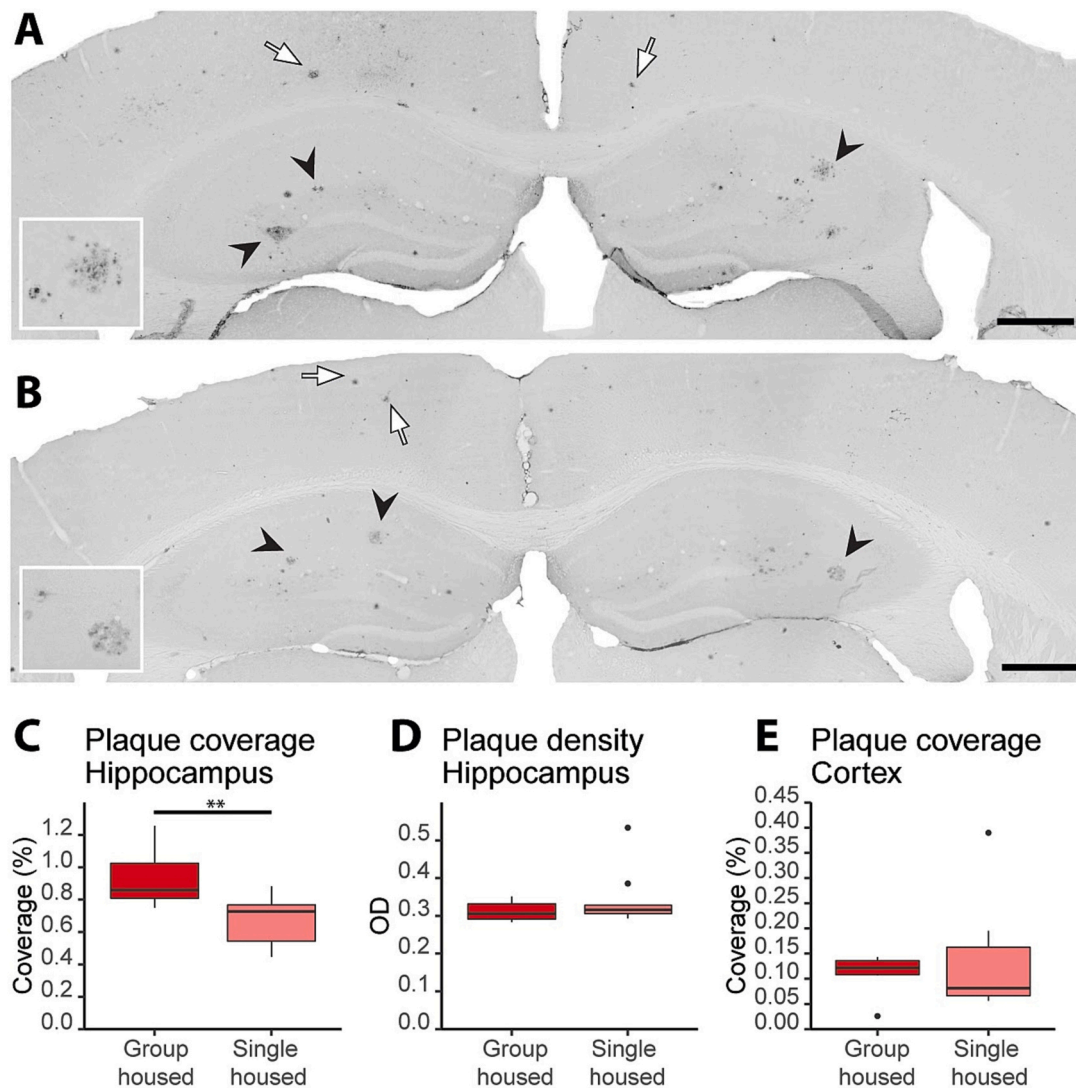
Fig. 2. *Plaque load.* Plaques in the cortex and hippocampus of a GH-J20 mouse at Bregma −1.55 (A) and SH-J20 mouse at Bregma −1.65 (B) visualized with 6e10 antibody. The staining and the analysis was performed on GH-WT mice ($n = 11$), SH-WT mice ($n = 12$), GH-J20 mice ($n = 10$), and SH-J20 mice (n = 12). Contrast and brightness have been enhanced for visualization purposes in these pictures only. The included sections were between Bregma −1.55 and - 2.35. Coverage in the cortex was measured in the cortical area above the hippocampus, spanning from +3–4 mm to −3 -4 mm (depending on the Bregma coordinate) relative to the A/P midline. Several plaques are indicated with arrows in the cortex (white arrows) and in the hippocampus (black arrowheads). Scale bar represents 500 μm. C-E) Boxplots indicating the IQR (box), median (black line), minimum and maximum value (whiskers), and statistical outliers (dots). Significant differences between groups are indicated with asterisks (*$p < 0.05$, **$p < 0.01$, ***$p < 0.001$). C) Mean plaque load (plaque coverage) in the hippocampus. GH-J20 mice have a higher plaque load compared to SH-J20 mice ($t_{(14)} = 3.099$, p = 0.007). D) Optical density (OD) of the detected plaques in the hippocampus is similar between group housed and single housed mice. E) Plaque load in the cortex did not differ between GH-J20 mice and SH-J20 mice.

3. Results

3.1. J20 mice

The sudden death rate of J20 mice (30%) was consistent with previously reported death rates and previous studies from our lab (Cheng et al., 2007; Gulbranson et al., 2021). The incidence of sudden death was higher among GH-J20 (41%) mice compared to SH-J20 mice (21%).

During cryosectioning, it was noticed that two brains of J20 mice exhibited corpus callosum dysgenesis. The corpus callosum fibers of these mice stopped to transverse the two hemispheres from Bregma −2.2 to caudal, while this normally starts around Bregma −2.7. Abnormalities of the anatomy of the corpus callosum related to genetic alterations of the hAPP gene have been described before (Magara et al., 1999; Müller et al., 1994; Sosa et al., 2017).

3.1.1. Reduced hippocampal amyloid-β plaque load in SH-J20 mice

Amyloid-β plaques were detected in all J20 mice, with the highest levels in the hippocampus (Fig. 2A+B). In the hippocampus, the plaque load (coverage) was higher in GH mice compared to SH mice (independent *t*-test: $t_{(14)} = 3.099$, $p = 0.007$) (Fig. 2C). The density of the plaques did not differ between groups (Wilcoxon rank sum test: $W = 21$, $p = 0.299$) (Fig. 2D). WT mice did not show plaques. In the cortical area above the hippocampus (encompassing the retrosplenial, somatosensory, and motor or parietal cortex), no difference in plaque load was detected (Wilcoxon rank sum test: $W = 23$, $p = 0.836$) (Fig. 2E).

3.1.2. Microglia number and morphology is affected by genotype

The hippocampus of both WT and J20 mice displayed the presence of many microglial cells (Fig. 3A-C). An overall effect of genotype was found on the number of microglia in the CA1 (linear model: $β[J20] = -0.02$, 95% CI [−0.04, −7.28e-03], $t_{(39)} = -2.91$, $p = 0.004$) and the DG (linear model: $β[J20] = 0.42$, 95% CI [0.29, 0.55], $t_{(39)} = 6.49$, $p < 0.001$), showing a small decrease of microglia in the CA1 of J20 mice but an increase in the DG (Fig. 3D and H, respectively). Post-hoc comparisons revealed that the number of microglia in the CA1 was only statistically lower in GH-J20 compared to GH-WT mice ($p = 0.0289$). In the DG, the number of microglia was higher in the J20 mice compared to the WT mice in the same housing condition (post-hoc comparison GH-WT vs GH-J20, $p < 0.001$; SH-WT vs SH-J20, $p < 0.001$).

Furthermore, the J20 genotype increased the microglia cell body to cell size ratio in the CA1 ($β[J20] = 0.01$, 95% CI [5.54e-03, 0.02], $t_{(37)} = 3.23$, $p = 0.003$) and the DG ($β[J20] = 0.05$, 95% CI [0.04, 0.06], $t_{(39)} = 7.49$, $p < 0.001$) (Fig. 3D and E). In addition, in the CA1, an effect of the housing condition ($β[SH]$ -0.01, 95% CI [−0.02, −3.08e-03], $t_{(37)} = -2.68$, $p = 0.011$) and an interaction effect between SH and genotype ($β = -0.02$, 95% CI [−0.03, −7.32e-03], $t_{(37)} = -3.20$, $p = 0.003$) was detected. Post-hoc comparison revealed a statistical difference between GH-WT and GH-J20 mice ($p = 0.013$) and a trend for an effect of the housing condition in J20 mice ($p = 0.051$).

Additional analysis revealed an effect of genotype in the cell body size and dendritic tree size of microglia in both the CA1 ($β[J20] = 23.38$, $p = 0.028$; $β[J20] = -887.3$, $p = 0.041$, resp.) and DG ($β[J20] = -59.34$, $p < 0.001$; $β[J20] = -1224.76$, $p < 0.001$, resp.). The social housing condition did not affect cell body size or dendritic tree size (Supplementary Fig. 2).

Coverage and optical density were not affected by genotype (CA1: Coverage $p = 0.108$, OD $p = 0.649$; DG: Coverage $p = 0.087$, OD $p = 0.427$) or housing condition (CA1: Coverage $p = 0.904$, OD $p = 0.996$; DG: Coverage $p = 0.784$, OD $p = 0.725$) in the CA1 (Fig. 3E and F) or DG (Fig. 3I and J).

3.1.3. Amyloid pathology is linked to shrinkage of the CA1 pyramidal cell layer

The thickness of the CA1 pyramidal cell layer was found to be lower for J20 mice compared to WT mice ($F = 14.172$, $p < 0.001$) (Fig. 4). No

effect of the housing condition ($p = 0.80$) or interaction effect between housing condition and genotype ($p = 0.78$) on pyramidal cell layer thickness was found. The number of cells was reduced in J20 mice compared to WT mice ($F = 7.20$, $p = 0.014$). The housing condition alone did not affect the number of cells ($p = 0.84$), and no interaction effect was found ($p = 0.085$).

3.2. B. P301L mice

3.2.1. Behavior

A large proportion of P301L mice displayed a hyperactive phenotype in their home cage. The majority of these mice developed stereotypic behavior (Fig. 5), mainly expressed as backward somersaulting and repetitive circling. Following the onset of stereotypic behavior in mice, its frequency either increased progressively or remained stable, with no instances of complete cessation observed. A Cox proportional hazard regression has been performed to assess the effect of the housing condition, the injection, and possible interaction between these two variables on the onset of stereotypic behavior. The hazard ratio for single housing was 2.54 (95% CI: 1.16–5.55, $p = 0.020$), indicating a significant positive association with the risk to develop stereotypic behavior. No significant effect of the injection was found ($p = 0.28$), and no interaction effect was found ($p = 0.50$). A post-hoc pairwise comparison using Log-Rank test with Bonferroni correction showed that only the SH-P301L$_{K18}$ and GH-P301L$_{PBS}$ significantly differed from each other ($p = 0.0027$). Next, it was assessed whether the survival curves differed from the moment of the injection by repeating the analysis on a dataset with the cases before the injection excluded. This analysis showed that from the moment of the PBS/K18 injection (12 weeks of age) the hazard ratio to develop stereotypic behavior was not influenced by the injected PBS or K18 ($p = 0.48$), and the effect of the housing was not accelerated by the injection of either PBS or K18 ($p = 0.30$).

Further analyses of the behavior of the P301L mice showed no distinct behavioral profile related to the housing condition or PBS/K18 injection in explorative behavior in the Open Field, motor performance on the accelerated Rotarod, alternation percentage in the Y-maze, or sociability in the Three Chamber Task (Supplementary Fig. 3).

The AT8 hyperphosphorylation score and the microglia activity did not differ between mice with and without stereotypic behavior, suggesting the stereotypic behavior did not influence these readouts (Supplementary Fig. 4 and 5).

3.2.2. AT8-immunoreactivity is unaffected by the housing condition

Strong AT8-positive staining was observed in the hippocampus and moderate positive staining in connected areas, including the anterior cingulate cortex, amygdala, entorhinal cortex, motor cortex, piriform cortex, retrosplenial cortex, and medial and lateral septum (Fig. 6A-D). A few mice also displayed some low positive staining (score 1) in the frontal cortex. The pattern of tau hyperphosphorylation was similar to that described by Peeraer et al. (2014) (Peeraer et al., 2014). AT8-positive tau staining in the contralateral hemisphere mirrored that of the ipsilateral hemisphere, while the ipsilateral hemisphere displayed higher AT8-immunoreactivity compared to the contralateral hemisphere (Fig. 7A-D). The strongest AT8-positive staining in the contralateral hemisphere of P301L$_{K18}$ mice was found in the hippocampus, yet this was not as strong as in the ipsilateral hippocampus (Fig. 7A and B).

Very mild AT8-immunoreactivity was observed in the brains of PBS injected animals, but this was not strong enough to meet the criteria for a score 1 or higher in any of the regions (Fig. 6E, 7C and D).

Semi-quantitative analysis of the ipsilateral side showed no difference between SH and GH mice in AT8-immunoreactivity in any of the investigated brain regions (Fig. 8).

Several mice ($n = 5$ in GH-P301L$_{K18}$ mice and $n = 6$ in SH-P301L$_{K18}$ mice) displayed positive staining in the thalamus nucleus directly beneath the injection location. This may have been the result from inserting the needle slightly too deep during the hippocampal injection,
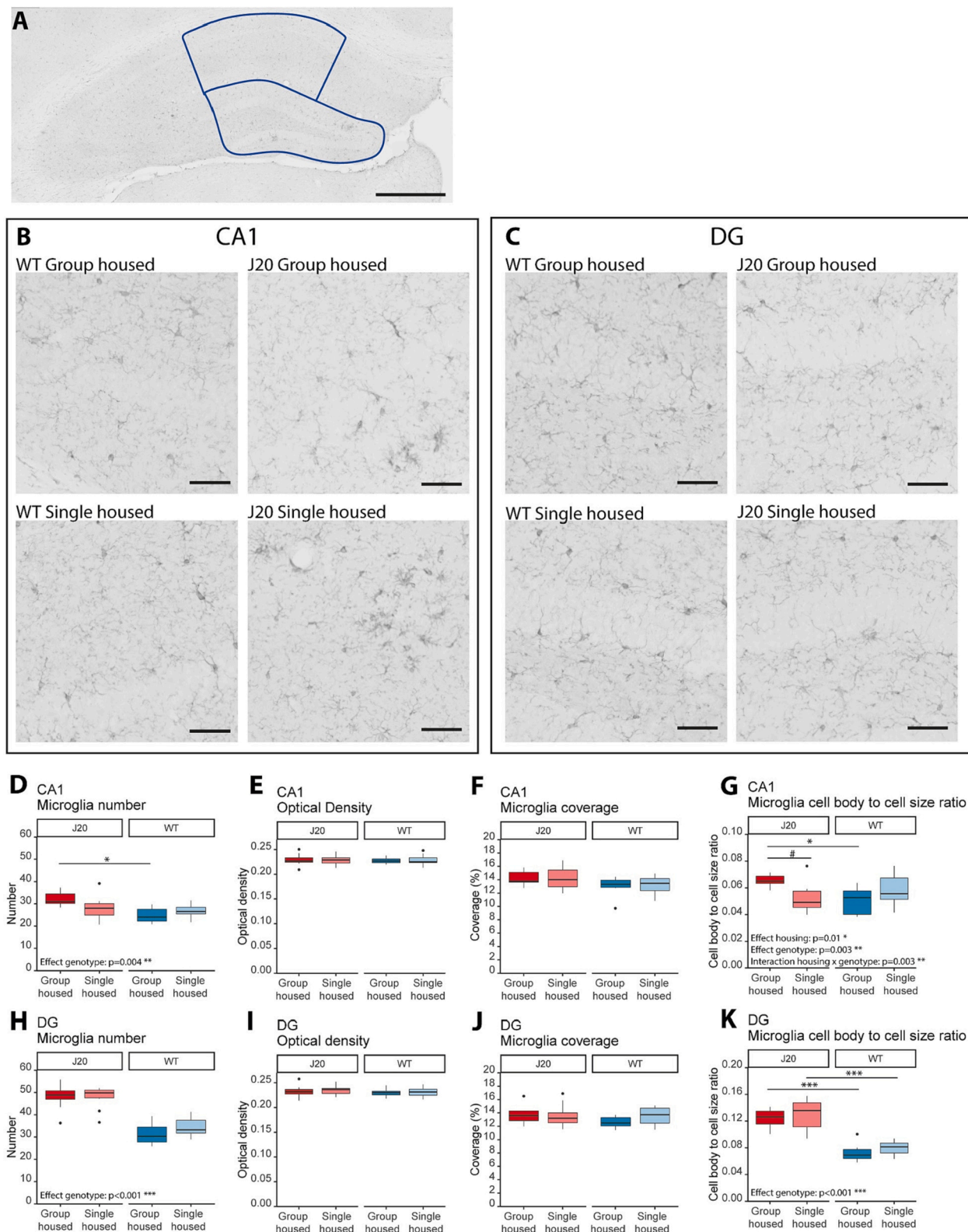
Fig. 3. Analysis of microglia on group housed J20 mice (*n* = 8), isolated J20 mice (*n* = 11), group housed WT mice (*n* = 10), isolated WT mice (*n* = 14). A) Representative image of a hippocampus of a GH-J20 mouse at Bregma −1.85. The blue areas indicate the ROI for the CA1 and DG analyses. The scale bar represents 500 μm. B + C) A close-up of microglia in the CA1 (B) and the DG (C) of the different experimental groups. Scale bars represent 50 μm. D–K) Panel of the results of the analysis of the CA1 (D-G) and DG (H–K) region. Microglia cell body to cell size ratio was affected by the social housing condition (CA1 and DG, panel G and K) and genotype (DG, panel K). Boxplots indicating the IQR (box), median (black line), minimum and maximum value (whiskers), and statistical outliers (dots). Significant differences between groups are indicated with asterisks (*$p < 0.05$, **$p < 0.01$, ***$p < 0.001$), a statistical trend is indicated with a dash (#$p = 0.05$–0.06). (For interpretation of the references to colour in this figure legend, the reader is referred to the web version of this article.)
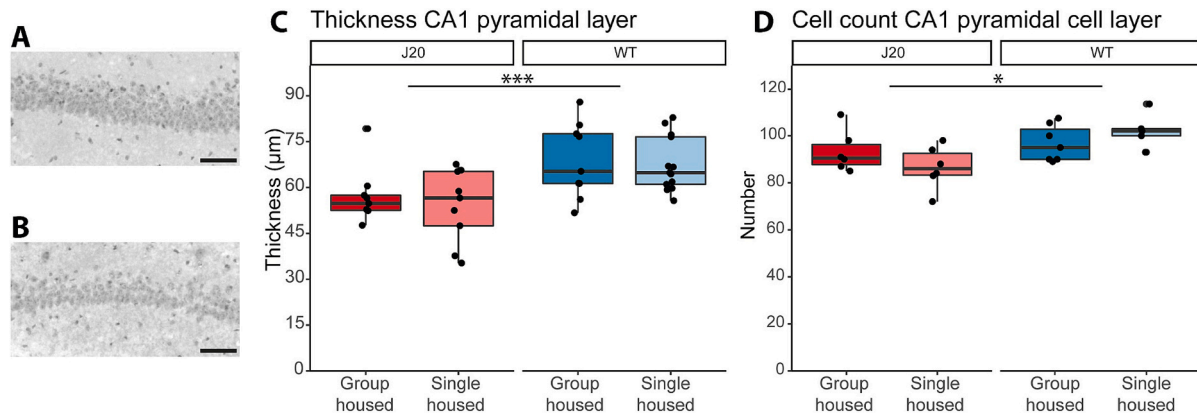
Fig. 4. *Analysis of the CA1 pyramidal cell layer of J20 mice.* A representative image of the pyramidal cell layer of a WT mouse (A) and a J20 mouse (B) are shown. The images were stained with hematoxylin. The analyzed sections were between Bregma −1.55 and - 2.35. Scale bars represent 50 μm. Boxplots indicate the IQR (box), median (black line), minimum and maximum value (whiskers), and all individual data points (dots). Significant differences between groups are indicated with asterisks ($*p < 0.05$, $**p < 0.01$, $***p < 0.001$). Group housed J20 mice ($n = 9$), isolated J20 mice ($n = 9$), group housed WT mice ($n = 9$), isolated WT mice ($n = 13$). C) The CA1 pyramidal cell layer was thicker in WT mice compared to J20 mice ($p < 0.001$), but unaffected by social isolation ($p = 0.80$). D) The number of cells in the cells in the CA1 pyramidal cell layer was lower in the J20 mice compared to the WT mice, but this number was not affected by the social housing condition.
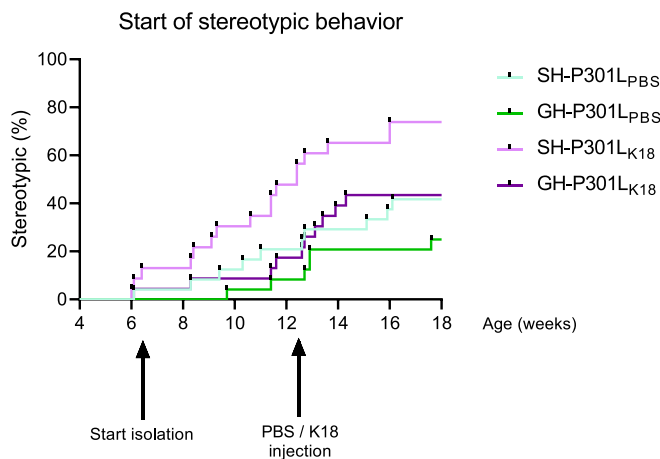
Fig. 5. *The onset of stereotypic behavior in P301L mice.* A survival plot displaying the onset of stereotypic behavior in each experimental group. The age (in weeks) when stereotypic behavior was first observed was considered as an event. The housing intervention started when mice were between 6 and 7 weeks of age. PBS or K18 was injected into the hippocampus when mice were 3 months old. The development of stereotypic behavior is associated with single housing (hazard ratio 2.54 (95% CI: 1.16–5.55, p = 0.020) but not with PBS/ K18 injection (p = 0.50).

or from proximity-based tau spread.

3.2.3. Altered morphology of microglia upon K18 injection, but not the social housing condition

At the age of 12 weeks, the social housing condition did not affect microglia number or cell body to cell size ratio in P301L mice of cohort 1 (Fig. 9).

The IBA1 immunostaining of hippocampi of mice from cohort 2 revealed a distinct microglia morphology and pattern in P301L$_{K18}$ mice, namely rod microglia (Taylor et al., 2014) (Fig. 10A-C)). These microglial cells present an elongated soma with retracted planar processes and elongated polar processes (Fig. 10C). These rod microglia aligned with the apical dendrites of the hippocampal CA1 neurons, forming 'trains'. This phenotype and pattern was most evident in the ipsilateral hemispheres of the P301L$_{K18}$ mice, where the majority of the microglia in the ipsilateral displayed this phenotype.

The social housing condition did not affect any of the microglia

readouts in the CA1 or DG (Fig. 10D-K). Seeding affected the number of microglia in the CA1 (β[K18] = 0.86, 95% CI [0.37, 1.34], t(28) = 3.62, p = 0.001) and DG (β[K18] = 0.83, 95% CI [0.22, 1.44], t(28) = 2.79, p = 0.009) (Fig. 10D + 10H). Post-hoc analyses revealed that in the CA1, GH-P301L$_{K18}$ and SH-P301L$_{K18}$ exhibited a higher number of microglia compared to GH-P301L$_{PBS}$ and SH-P301L$_{PBS}$, respectively (p = 0.006, p < 0.001, resp.). Similarly, in the DG, post-hoc comparison revealed a higher number of microglia in GH-P301L$_{K18}$ mice and SH-P301L$_{K18}$ mice compared to GH-P301L$_{PBS}$ mice and SH-P301L$_{PBS}$ mice, respectively (p = 0.044, p = 0.023, resp.) In addition, seeding increased the coverage of IBA1-positive area in the CA1 (β[K18] = 0.32, 95% CI [0.0047, 0.64], t (28) = 2.08, p = 0.047), with the strongest effect in SH-P301L mice (p < 0.001) (Fig. 10F). The OD remained unaffected by seeding with K18 (Fig. 10E and I).

Additional analysis of the microglia cell body size and dendritic tree size revealed no differences between the experimental groups (Supplementary Fig. 6). Furthermore, blood inflammatory markers were investigated, but no differences between the experimental groups were detected (Supplementary Fig. 7).

3.2.4. AD pathology is linked to CA1 pyramidal cell deterioration

The thickness of the CA1 pyramidal cell layer did not differ between groups and thus was not affected by the seeding or the social housing condition (Fig. 11A). Further analysis of the CA1 neurons on a different batch of brains did reveal the presence of degenerated and apoptotic neurons in the P301L$_{K18}$ brains but not in the P301L$_{PBS}$ brains (Fig. 11B-D). Furthermore, white matter integrity was not affected by housing. White matter tracts did not show any abnormalities in any of the groups (Fig. 11E). Thus, white matter integrity was not affected by seeding or single housing.

4. Discussion

In the current study, we investigated the effect of the social environment (social housing condition) on AD-related pathology (amyloid-β plaques or tau hyperphosphorylation, microglia activity (e.g., number and morphology), and CA1 neuronal cell death or CA1 cell layer thickness) by means of histological assessment in a two mouse models; J20 mice (a model for amyloid pathology) and P301L mice with K18 seeding (a model for tau propagation).

In both mouse models, we confirmed the presence of the model-specific AD-related pathology; Aβ plaques in J20 mice and widespread hyperphosphorylated tau in P301L$_{K18}$ mice. Additionally, changes were
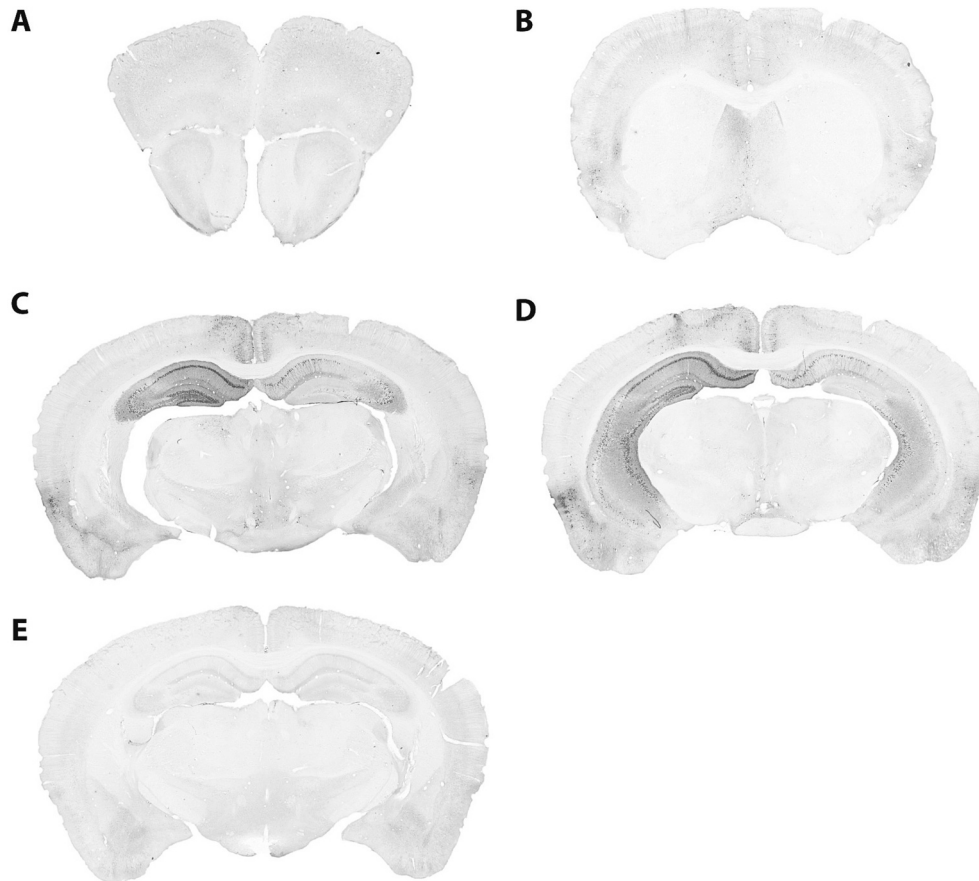
Fig. 6. Representative images of P301L$_{K18}$ brain sections stained with AT8. Fig. A-D are from the same P301L$_{K18}$ mouse. The ipsilateral hemisphere is displayed left. The contralateral hemisphere was marked with an incision in the cortex. Brightness and contrast levels were adjusted for visualization purposes. The injection site was located at Bregma −2.5. A) Frontal cortex section at Bregma 2.54. B) Striatal section at Bregma 1.05, used to assess staining in the anterior cingulate cortex, motor cortex, piriform cortex, and the medial and lateral septum. C) A dorsal hippocampal section at Bregma −2.15. D) A ventral hippocampal section at Bregma −2.55, with staining around the tract of the needle. E) Section of a P301L$_{PBS}$ mouse with very mild AT8 immunoreactivity in the hippocampus and amygdala at Bregma −2.15.

observed in the CA1 region of J20 (reduced number of cells and thickness of the layer) and P301L$_{K18}$ (neuronal death) mice. While no direct measures for neuronal cell death were applied in the J20 mouse line, the decreased thickness and reduced number of cells implies a combination of cell shrinkage and cell death in J20 mice. In both mouse lines, the CA1 readouts were unaffected by the housing condition.

Remarkably, in contrast to our hypothesis, J20 mice housed in groups displayed increased hippocampal plaque load. This is also in contradiction to previous findings showing increased hippocampal plaque load (Dong et al., 2004; Huang et al., 2015; Peterman et al., 2020) and Aβ40 and Aβ42 levels (Hsiao et al., 2011) in single housed mice. Other studies found similar levels in SH mice (Liang et al., 2019; Pietropaolo et al., 2009), but increased plaque load upon social isolation has not been reported before. Of note is that those studies used male mice (except (Pietropaolo et al., 2009)), different AD-mouse models, and examined different ages/disease stages. Importantly, the housing conditions of socially isolated and group housed mice described in the various studies also differ in important aspects, including the group composition of group housed mice (in number, age, and sex of cage mates) and the duration of the intervention. Collectively, these differences trouble the comparison with our results, but highlight that social environment under specific conditions do seem to affect AD-related pathology both in male and female mice.

It is well established from previous reports in both humans and mice that AD pathology differs between males and females (Zhu et al., 2021). For example, estrogen levels can influence the AD-induced cognitive decline (Uddin et al., 2020). Furthermore, the female hippocampus is more vulnerable to (social) stress which may accelerate amyloid pathology (Devi et al., 2010; Sotiropoulos et al., 2015). Additionally, sex differences in microglia number and reactivity have been identified (Han et al., 2021; Lynch, 2022). Sex could thus be an important determinant of the effect of an intervention. Only one mouse study included both genders when investigating the effect of social housing on AD-related behavior and reported a larger effect of sex compared to SH on APP-pathology (Pietropaolo et al., 2009). Increased plaque load upon social isolation has only been reported in male mice but not in female mice (Dong et al., 2004; Huang et al., 2015; Peterman et al., 2020). It is unclear whether this is a gender effect or a gender bias, since females are understudied in biomedical research.

Based on our data and in view of the relative paucity in literature on this topic, we can only speculate how group housing is associated with increased plaque load in our J20 mice. Importantly, a number of factors could underlie the observed results. For instance, group housing may have caused stress in the mice (Kamakura et al., 2016), thereby accelerating AD pathology (Devi et al., 2010; Sotiropoulos et al., 2015). For example, cage crowding can impose stress on the animals (Lin et al., 2015). However, the mean floor space per mouse in our study was comparable to several other studies (Dong et al., 2014), albeit smaller than the study of Peterman and Pietropaolo (Peterman et al., 2020; Pietropaolo et al., 2009). Furthermore, especially in sick animals, the inability to withdraw from a group (which is normal sickness behavior (Dantzer and Kelley, 2007; Kelley et al., 2003)) may cause (additional)
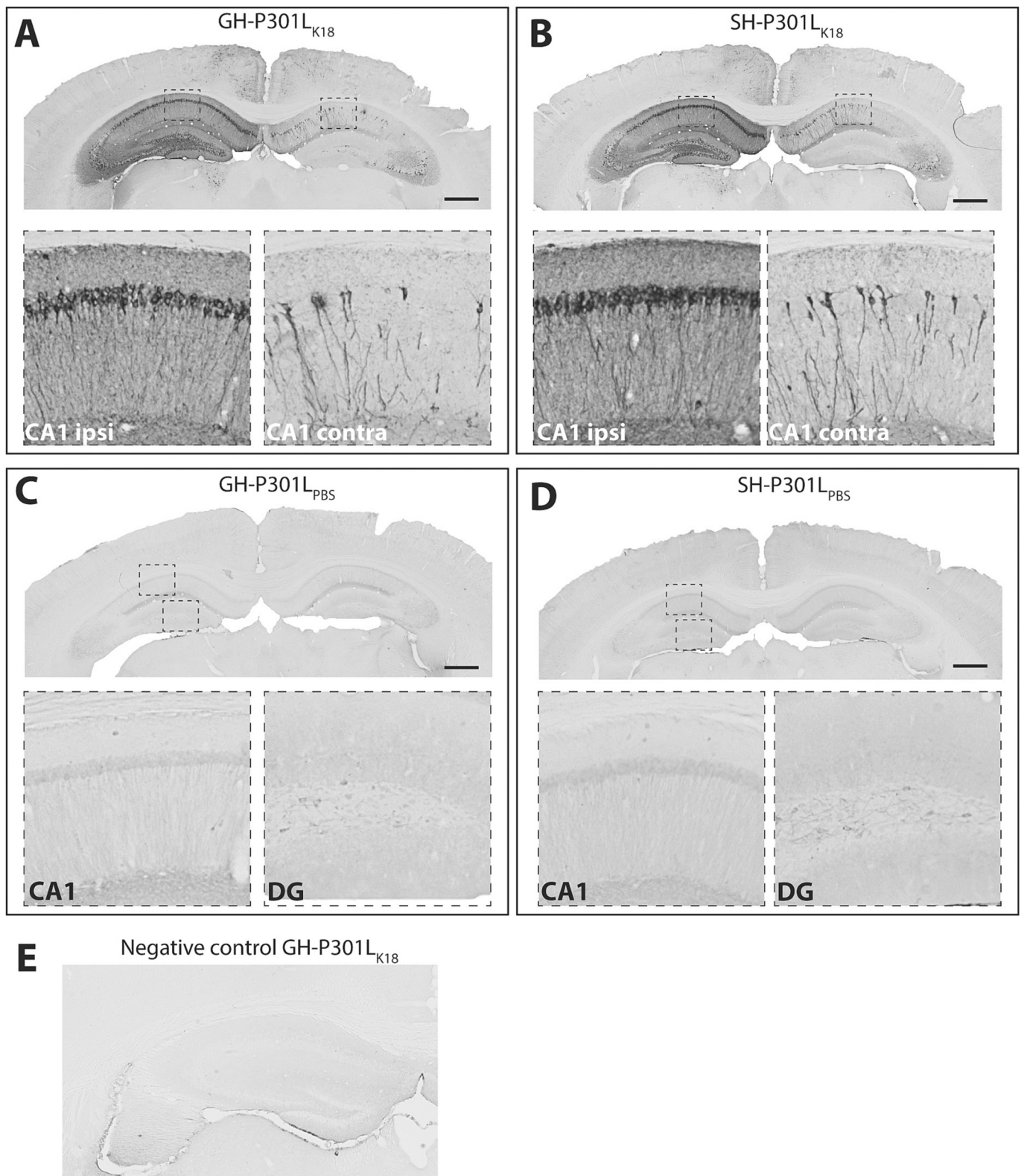
Fig. 7. *Hippocampal tau hyperphosphorylation visualized with anti-AT8 in 4-month old P301L mice (cohort 2).* Representative images of the hippocampus of a GH-P301LK18 mouse at Bregma −2.05 (A), SH-P301LK18 mouse at Bregma −2.05 (B), GH-P301L$_{PBS}$ mouse at Bregma −2.05, (C), and SH-P301L$_{PBS}$ mouse at Bregma −1.95 (D). Brightness and contrast levels were adjusted for visualization purposes. Scale bars represent 500 μm. The ipsilateral hippocampus is shown on the left, and the contralateral hippocampus on the right. Higher magnification insets of the ipsilateral (ipsi) and contralateral (contra) CA1 of P301L$_{K18}$ mice are shown (A + B). Weak AT8 staining is visible in the CA1 and DG of GH-P301L$_{PBS}$ (C) mice and SH-P301L$_{PBS}$ mice (D). E) Picture of the ipsilateral hippocampus of a P301L$_{K18}$ mouse, used as a negative control (no primary antibody added) for the AT8-immunostaining.
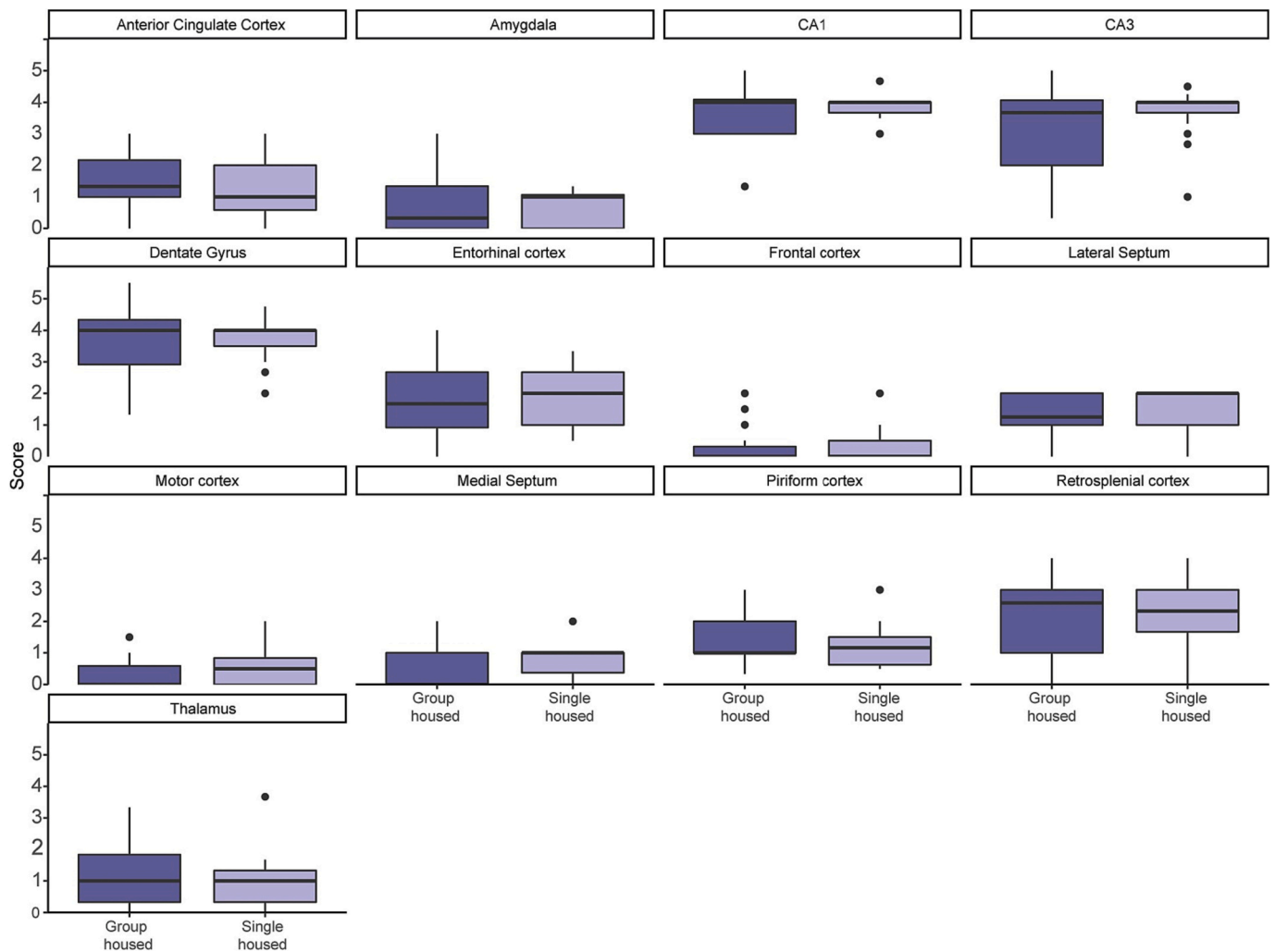
Fig. 8. *Boxplots of the semi-quantitative analysis of AT8-immunoreactivity in the ipsilateral hemisphere of SH-P301L $_{K18}$ (n = 21) and GH-P301L $_{K18}$ mice (n = 24)*. Boxplots indicate the IQR (box), median (black line), minimum and maximum value (whiskers), and statistical outliers (dots). No effect of the social housing condition was observed in any of these brain regions.

stress to an animal. However, no effect of the social housing condition on microglia activity was observed in the DG, while this region is especially susceptible to environmental changes. Instead, we found an effect of the housing condition and an interaction effect (genotype x housing) on microglia activation status (based on the cell body to cell size ratio) in the CA1 region. It has been well established that social housing conditions (e.g., social isolation) can modulate NMDA receptor expression (Mumtaz et al., 2018). Interestingly, microglia morphology correlates with the susceptibility of hippocampal subregions to NMDA-induced excitotoxicity (Howe and Barres, 2012; Vinet et al., 2012). The CA1 hippocampal subregion is most susceptible to NMDA-induced excitotoxicity and treatment of hippocampal slices with NMDA can result in increased microglia activation (Vinet et al., 2012). In contrast, in the DG, the neuroprotection against excitotoxicity is suggested to be mediated by ramified microglia rather than activated microglia (Vinet et al., 2012). This may explain the absence of an effect in the DG on microglia activation.

Furthermore, for the interpretation of our data, it should be noted that not the amyloid-β plaques but the soluble Aβ oligomers are most neurotoxic and correlate better with cognitive symptoms in AD patients (Haass and Selkoe, 2007; Mucke and Selkoe, 2012), although this relationship is less well established in mice (Foley et al., 2015). However, since cognitive or other behavioral tests were beyond the scope of the present study, no conclusions can be drawn on the functional

consequence of the increased plaque load. In addition, the underlying mechanism leading to increased plaque load (e.g., BACE activity) was not investigated. Thus, the underlying processes of the interplay between social housing conditions and APP-pathology in female mice require further investigation.

In the P301L mice, single housing was associated with the development of stereotypic behavior. These behaviors have been reported before in these tau-P301L mice (Detrez et al., 2020) and mice of the FVB background strain (Garner et al., 2004). Stereotypic behavior can develop under stressful conditions (Mason, 1991; Würbel and Stauffacher, 1997), but corticosterone reactivity and stereotypy levels do not necessarily correlate (Engel et al., 2011). While the staining results of the AT8 and IBA-1 staining did not differ between mice with and without stereotypic behavior, the stereotypic behavior may still have influenced our results. After all, a mouse without stereotypic behavior was always housed with mice expressing this behavior, and its/their presence may affect this mouse's behavior and physiology. For instance, the constant circling of a mouse and the possibly distorted social interaction may impose stress on the cage-mates and affect their physiology, possibly masking an effect of the hippocampal injection or housing condition. Yet, our data on the development of stereotypic behavior indicates that the social housing condition has the potential to modulate this behavior, but seems to have no effect on our AD-related histological readouts.

Unilateral K18 seeding resulted in widespread hyperphosphorylation
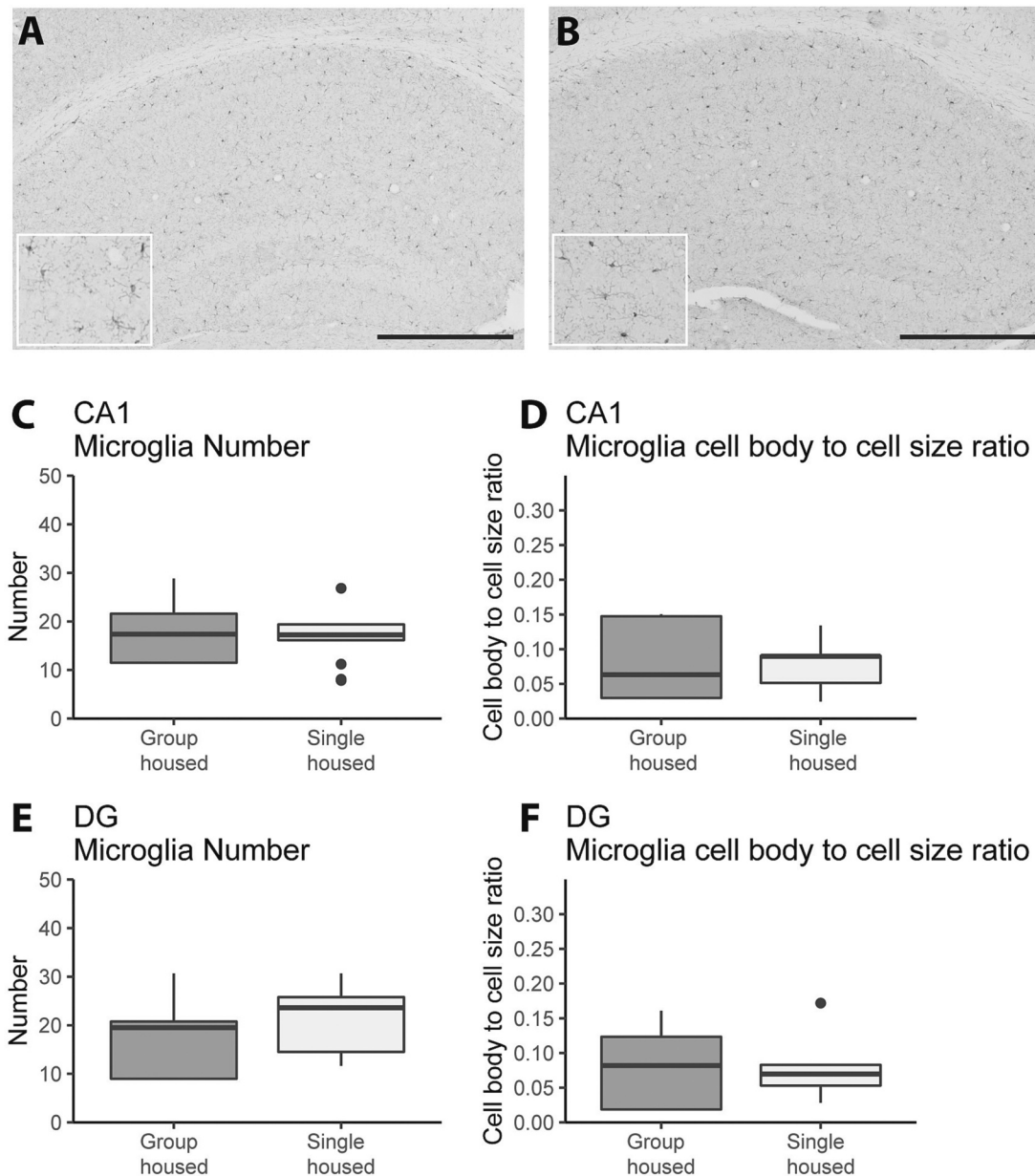
Fig. 9. *IBA1 staining in the hippocampus of 3-month-old P301L mice (cohort 1).* A representative image of the hippocampus of a GH-P301L mouse (A) and SH-P301L mouse (B) both at Bregma −1.85. A + B) Microglia morphology is displayed in more detail in the higher magnification insets. Scale bars represent 500 μm. Brightness and contrast levels were adjusted for visualization purposes. C–F) Boxplots indicate the IQR (box), median (black line), minimum and maximum value (whiskers), and statistical outliers (dots). Significant differences between groups are indicated with asterisks (*$p < 0.05$, **$p < 0.01$, ***$p < 0.001$). Microglia number and cell body to cell size ratio in the CA1 or DG did not differ between group housed mice and single housed mice.

of tau at site Ser202/Thr205 from the injection site to synaptically connected brain regions, including the contralateral hemisphere. The spread of tau aggregation from the injection site to synaptically connected brain regions is in line with findings of other studies using seeding mouse models, and in accordance with the theory that tau spreads in a 'prion-like' manner (Albert et al., 2019; Detrez et al., 2019; Holmes and Diamond, 2014; Kim et al., 2015). Yet, methodological differences (e.g., different injection coordinates, fibrils, or mouse model) may yield disparities in the spatiotemporal spread of tau. Nevertheless, our method was derived from the established experimental procedure used by Peeraer et al. (Peeraer et al., 2014), resulting in consistent findings. Without seeding, the P301L mice spontaneously develop tau pathology by the age of 9 months (Terwel et al., 2005), which corresponds to the very low AT8 immunoreactivity observed in our 4-month old P301L$_{PBS}$ mice.

Although strong hyperphosphorylation was observed in the CA1 of P301L$_{K18}$ mice, the consequence of this hyperphosphorylation on neuronal death was minor, which is in accordance with Peeraer et al. (Peeraer et al., 2014). No effect of the housing condition on CA1 neurodegeneration or tau pathology was detected. The effect of housing may be subtle, while the tau seeding caused strong AT8-immunoreactivity in the hippocampus, leaving no room for the detection of more subtle differences in immunoreactivity. Moreover, semi-quantitative analysis does not allow detection of subtle differences. Although additional and more detailed analyses could potentially reveal such subtle differences, the observation that the semi-quantitative analyses showed no differences in either the densely stained areas or the less densely stained ones makes it less likely that such subtle differences are present and can be detected. Furthermore, the hyperphosphorylation at Ser202/Thr205 is one of the earliest
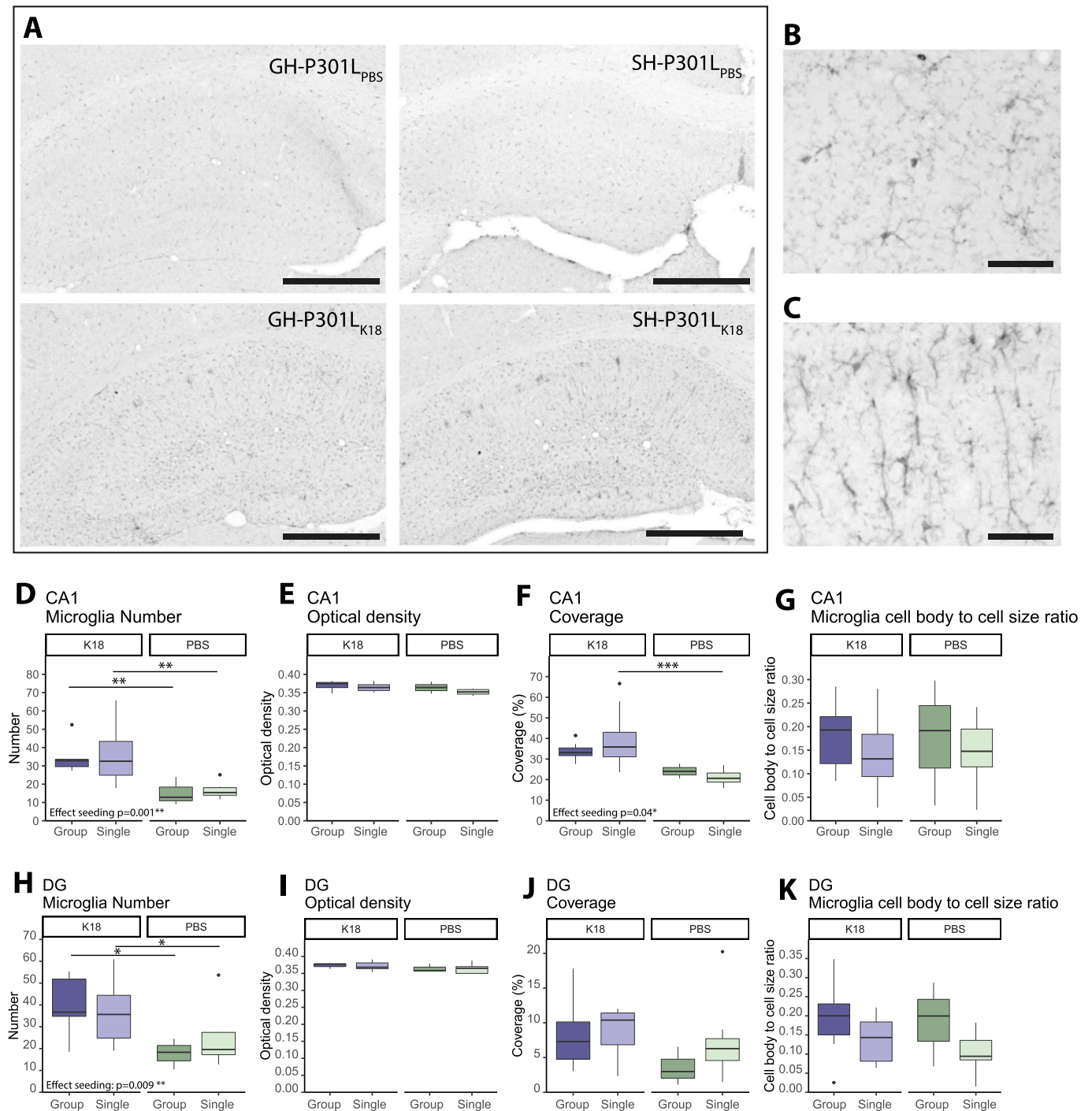
Fig. 10. *IBA1 staining in the hippocampus of 4-month-old P301L mice (cohort 2).* A) Representative images of the IBA1 staining showing microglia cells in the ipsilateral hippocampus of a mouse of each experimental group, taken at Bregma −1.85. B + C) Higher magnification picture of microglia in the CA1 of a GH-P301L$_{PBS}$ (B) and a GH-P301L$_{K18}$ mouse (C). Scale bars represent 500 μm (A) and 50 μm (B + C). Image contrast was enhanced to improve visualization. D-G) Results of the analysis in the CA1. The number of microglia was increased upon K18 seeding (p = 0.001). Post-hoc analyses revealed that GH-P301L$_{K18}$ and SH-P301L$_{K18}$ exhibited a higher number of microglia compared to GH-P301L$_{PBS}$ and SH-P301L$_{PBS}$, respectively (p = 0.006, p < 0.001, resp.) IBA1 coverage was enhanced by seeding (p = 0.047) and was significantly higher in SH-P301L$_{K18}$ mice compared to SH-P301L$_{PBS}$ mice (p < 0.001). H–K) Results of the analysis in the dentate gyrus. The number of microglia was increased upon K18 seeding (p = 0.009). Post-hoc comparison revealed a higher number of microglia in GH-P301L$_{K18}$ mice and SH-P301L$_{K18}$ mice compared to GH-P301L$_{PBS}$ mice and SH-P301L$_{PBS}$ mice, respectively (p = 0.044, p = 0.023, resp.) The social housing condition did not affect our microglia readouts. Boxplots indicate the IQR (box), median (black line), minimum and maximum value (whiskers), and statistical outliers (dots). Significant differences between groups are indicated with asterisks (*p < 0.05, **p < 0.01, ***p < 0.001).
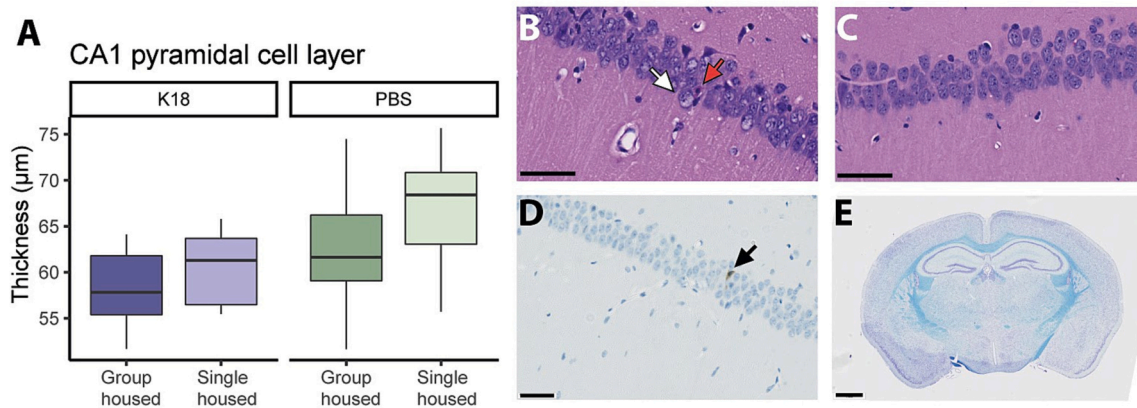
Fig. 11. *Histological analysis of the CA1 of 4-month-old P301L mice (A: cohort 2; B-E: cohort 3).* The boxplot indicates the IQR (box), median (black line), and minimum and maximum value (whiskers). Significant differences between groups are indicated with asterisks (*p < 0.05, **p < 0.01, ***p < 0.001). Hematoxylin staining (A-C). A) The thickness of the CA1 pyramidal cell layer did not differ between groups. B) P301L$_{K18}$ brain sections displayed several degenerating neurons with swollen vesicular nuclei (white arrow) and few apoptotic neurons (red arrow). C) A P301L$_{PBS}$ brain with histologically appearing normal neurons. D) Rare caspase-3 positive CA1 hippocampal neurons were present in the both SH-P301L$_{K18}$ and GH-P301L$_{K18}$ brains. E) Luxol fast blue staining with Cresyl Violet showed no abnormalities in myelin contents or myelin integrity in mice of any of the groups. Scale bars represent 50 μm (B–D) and 1000 μm (E). (For interpretation of the references to colour in this figure legend, the reader is referred to the web version of this article.)

phosphorylation sites. Quantitative analyses of additional markers for tau hyperphosphorylation sites affected at later stages (e.g., AT100, AT180) may provide additional insights into the progression of tau pathology in the GH- and SH-P301L mice.

The social housing condition had a limited effect on the microglia in J20 mice, and no effect on the microglia in P301L mice. Others have reported more pronounced effects of social isolation on microglia in AD mouse models (Huang et al., 2015). Yet, in healthy mice, social isolation has been found to both increase (Du Preez et al., 2021) and decrease (Du Preez et al., 2020) microglia activity. However, the vast majority of the detected microglia in our mice displayed ramification rather than a reactive profile, suggesting that these brains have not reached a stage of neuroinflammation yet. In this stage, microglia may serve a protective role in the AD pathogenesis (Odfalk et al., 2022). Moreover, our SH mice may not experience psychosocial stress as a consequence of the individual housing, because they were still able to smell, hear, and see other mice in the holding room (Piirainen et al., 2017). Furthermore, it should be noted that no distinction was made between plaque-associated microglia and non-plaque-associated microglia. Thus, the observed difference in microglia number in J20 mice compared to WT mice could be attributed to local increases in plaque-associated microglia. Follow-up studies could further assess the level of neuroinflammation by investigating the microglia profile in more detail by distinguishing between plaque- and non-plaque-associated microglia, using additional markers (e.g., CD68, TMEM119), or by investigating the cytokine profile (Minett et al., 2016; Ruan and Elyaman, 2022).

The rod microglia phenotype was the dominant microglia phenotype in the ipsilateral CA1 of the P301L$_{K18}$ mice. While microglia morphology relates to its function, the role of rod microglia remains poorly understood. Yet, these microglia are considered a form of activated microglia as they have been associated with brain damage and disease (Giordano et al., 2021). In addition, a few studies have described the presence of rod microglia in the hippocampus of AD-mouse models (Holloway et al., 2020; Perea et al., 2022) and K18-seeded mice (Detrez et al., 2019), but their function in AD disease progression remains unclear.

Considering our exploratory findings and the current literature, we advocate that alterations in the social environment have the potential to modulate AD-related pathology. Yet, the exact relationship between the social environment, AD pathology and the additional factors (e.g., sex) contributing to this relationship requires further investigation. The strength of this study is that we investigated two animal models for AD pathology, namely one addressing amyloid and another one addressing tau pathology. There were also limitations to this study. First, the investigation of only one age for each mouse model provided only limited information on how the social environment could affect the onset and progression of AD-related pathology. Second, while we have identified an effect of the social environment in both the amyloid model and the tau model, only a limited number of outcome measures were included in this study. Further studies including different time-points and readouts (e.g. biochemical fractions of soluble beta-amyloid or tau, or factors controlling beta-amyloid deposition) in both males and females are required to determine if amyloid pathology and tau pathology are differentially affected by social environmental manipulations. It will also be important to highlight that obtaining additional behavioral data related to learning and memory would be useful to further understand the impact of the social environment on AD related pathology in the cognitive domain. Increased understanding of the complex relationship between social factors and the brain in relation to AD and other forms of dementia may eventually contribute to our understanding of the applicability of social interventions focusing on preventing and delaying neurodegeneration (Lanooij et al., 2023).

Supplementary data to this article can be found online at https://doi.org/10.1016/j.nbd.2023.106309.

CRediT authorship contribution statement

Suzanne D. Lanooij: Conceptualization, Investigation, Formal analysis, Visualization, Writing – original draft. **W.H.I.M. Drinkenburg:** Conceptualization, Resources, Writing – review & editing. **U.L.M. Eisel:** Conceptualization, Writing – review & editing. **E.A. van der Zee:** Conceptualization, Writing – review & editing. **Martien J.H. Kas:** Conceptualization, Supervision, Funding acquisition, Writing – review & editing.

Declaration of Competing Interest

The authors declare no conflict of interest.

Data availability

Data will be made available on request.

References

Albert, M., Mairet-Coello, G., Danis, C., Lieger, S., Caillierez, R., Carrier, S., Skrobala, E., Landrieu, I., Michel, A., Schmitt, M., Citron, M., Downey, P., Courade, J.P., Buée, L., Colin, M., 2019. Prevention of tau seeding and propagation by immunotherapy with a central tau epitope antibody. Brain 142, 1736–1750. https://doi.org/10.1093/brain/awz100.

Ameen-Ali, K.E., Simpson, J.E., Wharton, S.B., Heath, P.R., Sharp, P.S., Brezzo, G., Berwick, J., 2019. The time course of recognition memory impairment and glial pathology in the hAPP-J20 mouse model of Alzheimer's disease. J. Alzheimers Dis. 68, 609–624. https://doi.org/10.3233/JAD-181238.

Bianchi, M., Fone, K.F.C., Azmi, N., Heidbreder, C.A., Hagan, J.J., Marsden, C.A., 2006. Isolation rearing induces recognition memory deficits accompanied by cytoskeletal alterations in rat hippocampus. Eur. J. Neurosci. 24, 2894–2902. https://doi.org/10.1111/j.1460-9568.2006.05170.x.

Bloom, G.S., 2014. Amyloid-β and tau: the trigger and bullet in Alzheimer disease pathogenesis. JAMA Neurol. 71, 505–508. https://doi.org/10.1001/jamaneurol.2013.5847.

Braak, H., Braak, E., 1991. Neuropathological stageing of Alzheimer-related changes. Acta Neuropathol. 82, 239–259.

Busche, M.A., Hyman, B.T., 2020. Synergy between amyloid-β and tau in Alzheimer's disease. Nat. Neurosci. 23, 1183–1193. https://doi.org/10.1038/s41593-020-0687-6.

Cheng, I.H., Scearce-Levie, K., Legleiter, J., Palop, J.J., Gerstein, H., Bien-Ly, N., Puoliväli, J., Lesné, S., Ashe, K.H., Muchowski, P.J., Mucke, L., 2007. Accelerating amyloid-β fibrillization reduces oligomer levels and functional deficits in Alzheimer disease mouse models. J. Biol. Chem. 282, 23818–23828. https://doi.org/10.1074/jbc.M701618200.

Dani, M., Wood, M., Mizoguchi, R., Fan, Z., Walker, Z., Morgan, R., Hinz, R., Biju, M., Kuruvilla, T., Brooks, D.J., Edison, P., 2018. Microglial activation correlates in vivo with both tau and amyloid in Alzheimer's disease. Brain 141, 2740–2754. https://doi.org/10.1093/brain/awy188.

Dantzer, R., Kelley, K.W., 2007. Twenty Years of Research on Cytokine-Induced Sickness Behavior, 21, pp. 153–160. https://doi.org/10.1016/j.bbi.2006.09.006.

Detrez, J.R., Maurin, H., Van Kolen, K., Willems, R., Colombelli, J., Lechat, B., Roucourt, B., Van Leuven, F., Baatout, S., Larsen, P., Nuydens, R., Timmermans, J.P., De Vos, W.H., 2019. Regional vulnerability and spreading of hyperphosphorylated tau in seeded mouse brain. Neurobiol. Dis. 127, 398–409. https://doi.org/10.1016/j.nbd.2019.03.010.

Detrez, J.R., Ben-Nejma, I.R.H., Van Kolen, K., Van Dam, D., De Deyn, P.P., Fransen, E., Verhoye, M., Timmermans, J.P., Nuydens, R., Van der Linden, A., Keliris, G.A., De Vos, W.H., 2020. Progressive tau aggregation does not alter functional brain network connectivity in seeded hTau.P301L mice. Neurobiol. Dis. 143, 105011. https://doi.org/10.1016/j.nbd.2020.105011.

Devi, L., Alldred, M.J., Ginsberg, S.D., Ohno, M., 2010. Sex- and brain region-specific acceleration of β-amyloidogenesis following behavioral stress in a mouse model of Alzheimer's disease. Mol. Brain. 3, 34. https://doi.org/10.1186/1756-6606-3-34.

Dong, H., Goico, B., Martin, M., Csernansky, C.A., Bertchume, A., Csernansky, J.G., 2004. Modulation of hippocampal cell proliferation, memory, and amyloid plaque deposition in APPsw (Tg2576) mutant mice by isolation stress. Neuroscience 127, 601–609. https://doi.org/10.1016/j.neuroscience.2004.05.040.

Dong, H., Wang, S., Zeng, Z., Li, F., Montalvo-Ortiz, J., Tucker, C., Akhtar, S., Shi, J., Meltzer, H.Y., Rice, K.C., Csernansky, J.G., 2014. Effects of corticotrophin-releasing factor receptor 1 antagonists on amyloid-β and behavior in Tg2576 mice. Psychopharmacology 231, 4711–4722. https://doi.org/10.1007/s00213-014-3629-8.

Du Preez, A., Law, T., Onorato, D., Lim, Y., Eiben, P., Musaelyan, K., Egeland, M., Hye, A., Zunszain, P., Thuret, S., Pariante, C., Fernandes, C., 2020. The type of stress matters: repeated injection and permanent social isolation stress in male mice have a differential effect on anxiety- and depressive-like behaviours, and associated biological alterations. Transl. Psychiatry 10.

Du Preez, A., Onorato, D., Eiben, I., Musaelyan, K., Egeland, M., Zunszain, P., Fernandes, C., Thuret, S., Pariante, C., 2021. Chronic stress followed by social isolation promotes depressive-like behaviour, alters microglial and astrocyte biology

and reduces hippocampal neurogenesis in male mice. Brain Behav. Immun. 91, 24–47.

ElAli, A., Rivest, S., 2016. Microglia in Alzheimer's disease: a multifaceted relationship. Brain Behav. Immun. 55, 138–150. https://doi.org/10.1016/j.bbi.2015.07.021.

Engel, A.K.J., Gross, A.N., Richter, S.H., Rommen, J., Touma, C., Würbel, H., 2011. Variation in stress reactivity affects cage-induced stereotypies in female CD-1 (ICR) mice. Appl. Anim. Behav. Sci. 133, 101–108. https://doi.org/10.1016/j.applanim.2011.04.017.

Evans, I.E.M., Llewellyn, D.J., Matthews, F., Woods, B., Brayne, C., Clare, L., 2018. Social isolation, cognitive reserve, and cognition in older people with mental health problems. PLoS One 13. https://doi.org/10.1371/journal.pone.0201008 A.

Fleck, J.I., Arnold, M., Dykstra, B., Casario, K., Douglas, E., Morris, O., 2019. Distinct functional connectivity patterns are associated with social and cognitive lifestyle factors: pathways to cognitive reserve. Front. Aging Neurosci. 11, 1–15. https://doi.org/10.3389/fnagi.2019.00310.

Foley, A.M., Ammar, Z.M., Lee, R.H., Mitchell, C.S., 2015. Systematic review of the relationship between amyloid-β levels and measures of transgenic mouse cognitive deficit in Alzheimer's disease. J. Alzheimers Dis. 44, 787–795. https://doi.org/10.3233/JAD-142208.

Garner, J.P., Dufour, B., Gregg, L.E., Weisker, S.M., Mench, J.A., 2004. Social and husbandry factors affecting the prevalence and severity of barbering ("whisker trimming") by laboratory mice. Appl. Anim. Behav. Sci. https://doi.org/10.1016/j.applanim.2004.07.004.

Giordano, K.R., Denman, C.R., Dubisch, P.S., Akhter, M., Lifshitz, J., 2021. An update on the rod microglia variant in experimental and clinical brain injury and disease. Brain Commun. 3 https://doi.org/10.1093/braincomms/fcaa227.

Gulbranson, D.R., Ho, K., Yu, G.Q., Yu, X., Das, M., Shao, E., Kim, D., Zhang, W.J., Choudhary, K., Thomas, R., Mucke, L., 2021. Phenotypic differences between the alzheimer's disease-related happ-j20 model and heterozygous zbtb20 knock-out mice. eNeuro 8. https://doi.org/10.1523/ENEURO.0089-21.2021.

Haass, C., Selkoe, D.J., 2007. Soluble protein oligomers in neurodegeneration: lessons from the Alzheimer's amyloid β-peptide. Nat. Rev. Mol. Cell Biol. 8, 101–112. https://doi.org/10.1038/nrm2101.

Hall, F.S., 1998. Social deprivation of neonatal, adolescent, and adult rats has distinct neurochemical and behavioral consequences. Crit. Rev. Neurobiol. 12 (1–2), 129–162.

Han, J., Fan, Y., Zhou, K., Blomgren, K., Harris, R.A., 2021. Uncovering sex differences of rodent microglia. J. Neuroinflammation 18, 1–11. https://doi.org/10.1186/s12974-021-02124-z.

Holloway, O.G., King, A.E., Ziebell, J.M., 2020. Microglia demonstrate local mixed inflammation and a defined morphological shift in an APP/PS1 mouse model. J. Alzheimers Dis. 77, 1765–1781. https://doi.org/10.3233/JAD-200098.

Holmes, B.B., Diamond, M.I., 2014. Prion-like properties of tau protein: the importance of extracellular tau as a therapeutic target. J. Biol. Chem. 289, 19855–19861. https://doi.org/10.1074/jbc.R114.549295.

Hovens, I., Nyakas, C., Schoemaker, R., 2014. A novel method for evaluating microglial activation using ionized calcium-binding adaptor protein-1 staining: cell body to cell size ratio. Neuroimmunol. Neuroinflammation 1, 82. https://doi.org/10.4103/2347-8659.139719.

Howe, M.L., Barres, B.A., 2012. A novel role for microglia in minimizing excitotoxicity. BMC Biol. 10, 2–4. https://doi.org/10.1186/1741-7007-10-7.

Hsiao, Y.H., Chen, P.S., Chen, S.H., Gean, P.W., 2011. The involvement of Cdk5 activator p35 in social isolation-triggered onset of early alzheimers disease-related cognitive deficit in the transgenic mice. Neuropsychopharmacology 36, 1848–1858. https://doi.org/10.1038/npp.2011.69.

Huang, H., Wang, L., Cao, M., Marshall, C., Gao, J., Xiao, Na, Hu, G., Xiao, Ming, Xiao, N., Xiao, M., 2015. Isolation housing exacerbates Alzheimer's disease- like pathophysiology in aged APP/PS1 mice. Int. J. Neuropsychopharmacol. 18, 1–10. https://doi.org/10.1093/ijnp/pyu116.

ImageJ.nig.gov, n.d. Optical Density Calibration [WWW Document]. URL https://imagej.nih.gov/ij/docs/examples/calibration/#:%E2%88%BC:text=The tablet has 21 steps,Tiffen (Kodak) and Stouffer.

Jaworski, T., Lechat, B., Demedts, D., Gielis, L., Devijver, H., Borghgraef, P., Duimel, H., Verheyen, F., Kügler, S., Van Leuven, F., 2011. Dendritic degeneration, neurovascular defects, and inflammation precede neuronal loss in a mouse model for tau-mediated neurodegeneration. Am. J. Pathol. 179, 2001–2015. https://doi.org/10.1016/j.ajpath.2011.06.025.

Kamakura, R., Kovalainen, M., Leppäluoto, J., Herzig, K.-H., Mäkelä, K.A., 2016. The effects of group and single housing and automated animal monitoring on urinary corticosterone levels in male C57BL/6 mice. Phys. Rep. 4 https://doi.org/10.14814/phy2.12703.

Kelley, K.W., Bluth, R., Dantzer, R., Zhou, J., Shen, W., Johnson, R.W., Broussard, S.R., 2003. Cytokine-induced sickness behavior. Brain Behav. Immun. 17, 112–118.

Kim, D., Lim, S., Haque, M.M., Ryoo, N., Hong, H.S., Rhim, H., Lee, D.E., Chang, Y.T., Lee, J.S., Cheong, E., Kim, D.J., Kim, Y.K., 2015. Identification of disulfide cross-linked tau dimer responsible for tau propagation. Sci. Rep. 5, 1–10. https://doi.org/10.1038/srep15231.

Kuznetsova, A., Brockhoff, P.B., Christensen, R.H.B., 2017. lmerTest package: tests in linear mixed effects models. J. Stat. Softw. 82, 1–26. https://doi.org/10.18637/JSS.V082.I13.

Lakshmisha Rao, Y., Ganaraja, B., Murlimanju, B.V., Joy, T., Krishnamurthy, A., Agrawal, A., 2022. Hippocampus and its involvement in Alzheimer's disease: a review. 3 Biotech. 12, 1–10. https://doi.org/10.1007/s13205-022-03123-4.

Lander, S.S., Linder-Shacham, D., Gaisler-Salomon, I., 2017. Differential effects of social isolation in adolescent and adult mice on behavior and cortical gene expression. Behav. Brain Res. 316, 245–254. https://doi.org/10.1016/j.bbr.2016.09.005.

Lanooij, S.D., Eisel, U.L.M., Drinkenburg, W.H.I.M., van der Zee, E.A., Kas, M.J.H., 2023. Influencing cognitive performance via social interactions: a novel therapeutic approach for brain disorders based on neuroanatomical mapping? Mol. Psychiatry 28, 28–33. https://doi.org/10.1038/s41380-022-01698-1.

Lenart-Bugla, M., Łuc, M., Pawłowski, M., Szcześniak, D., Seifert, I., Wiegelmann, H., Gerhardus, A., Wolf-Ostermann, K., Rouwette, E.A.J.A., Ikram, M.A., Brodaty, H., Jeon, Y.H., Maddock, J., Marseglia, A., Melis, R.J.F., Samtani, S., Wang, H.X., Welmer, A.K., Vernooij-Dassen, M., Rymaszewska, J., 2022. What do we know about social and non-social factors influencing the pathway from cognitive health to dementia? A systematic review of reviews. Brain Sci. 12 https://doi.org/10.3390/brainsci12091214.

Leng, F., Edison, P., 2021. Neuroinflammation and microglial activation in Alzheimer disease: where do we go from here? Nat. Rev. Neurol. 17, 157–172. https://doi.org/10.1038/s41582-020-00435-y.

Liang, F., Yang, S., Zhang, Y., Hao, T., 2019. Social housing promotes cognitive function through enhancing synaptic plasticity in APP/PS1 mice. Behav. Brain Res. 368, 111910. https://doi.org/10.1016/j.bbr.2019.111910.

Lin, E.-J.D., Sun, M., Choi, E.Y., Magee, D., Stets, C.W., During, M.J., 2015. Social overcrowding as a chronic stress model that increases adiposity in mice. Psychoneuroendocrinology 51, 318–330. https://doi.org/10.1016/j.psyneuen.2014.10.007.Social.

Lynch, M.A., 2022. Exploring sex-related differences in microglia may be a game-changer in precision medicine. Front. Aging Neurosci. 14, 1–17. https://doi.org/10.3389/fnagi.2022.868448.

Magara, F., Müller, U., Li, Z.W., Lipp, H.P., Weissmann, C., Stagljar, M., Wolfer, D.P., 1999. Genetic background changes the pattern of forebrain commissure defects in transgenic mice underexpressing the β-amyloid-precursor protein. Proc. Natl. Acad. Sci. U. S. A. 96, 4656–4661. https://doi.org/10.1073/pnas.96.8.4656.

Mason, G.J., 1991. Stereotypies: a critical review. Anim. Behav. 41, 1015–1037.

McRae, I., Zheng, L., Bourke, S., Cherbuin, N., Anstey, K.J., 2021. Cost-effectiveness of dementia prevention interventions. J. Prev. Alzheimer's Dis. 8, 210–217. https://doi.org/10.14283/jpad.2020.71.

Medendorp, W.E., Petersen, E.D., Pal, A., Wagner, L.M., Myers, A.R., Hochgeschwender, U., Jenrow, K.A., 2018. Altered behavior in mice socially isolated during adolescence corresponds with immature dendritic spine morphology and impaired plasticity in the prefrontal cortex. Front. Behav. Neurosci. 12, 1–13. https://doi.org/10.3389/fnbeh.2018.00087.

Minett, T., Classey, J., Matthews, F.E., Fahrenhold, M., Taga, M., Brayne, C., Ince, P.G., Nicoll, J.A.R., Boche, D., Cfas, M.R.C., 2016. Microglial immunophenotype in dementia with Alzheimer ' s pathology. J. Neuroinflammation 13, 1–10. https://doi.org/10.1186/s12974-016-0601-z.

Mucke, L., Selkoe, D.J., 2012. Neurotoxicity of amyloid β-protein: synaptic and network dysfunction. Cold Spring Harb. Perspect. Med. 2, 1–18. https://doi.org/10.1101/cshperspect.a006338.

Mucke, L., Masliah, E., Yu, G.Q., Mallory, M., Rockenstein, E.M., Tatsuno, G., Hu, K., Kholodenko, D., Johnson-Wood, K., McConlogue, L., 2000. High-level neuronal expression of abeta 1-42 in wild-type human amyloid protein precursor transgenic mice: synaptotoxicity without plaque formation. J. Neurosci. 20, 4050–4058. Doi: 20/11/4050 pii.

Mudher, A., Colin, M., Dujardin, S., Medina, M., Dewachter, I., Maryam, S., Naini, A., Mandelkow, E.-M., Mandelkow, E., Buée, L., Goedert, M., Brion, J., 2017. What is the evidence that tau pathology spreads through prion-like propagation ? Acta Neuropathol. Commun. 5, 1–20. https://doi.org/10.1186/s40478-017-0488-7.

Müller, U., Cristina, N., Li, Z.W., Wolfer, D.P., Lipp, H.P., Rülicke, T., Brandner, S., Aguzzi, A., Weissmann, C., 1994. Behavioral and anatomical deficits in mice homozygous for a modified β-amyloid precursor protein gene. Cell 79, 755–765. https://doi.org/10.1016/0092-8674(94)90066-3.

Mumtaz, F., Khan, M.I., Zubair, M., Dehpour, A.R., 2018. Neurobiology and consequences of social isolation stress in animal model—a comprehensive review. Biomed. Pharmacother. 105, 1205–1222. https://doi.org/10.1016/j.biopha.2018.05.086.

Odfalk, K.F., Bieniek, K.F., Hopp, S.C., 2022. Microglia: friend and foe in tauopathy. Prog. Neurobiol. 102306 https://doi.org/10.1016/j.pneurobio.2022.102306.

Peeraer, E., Bottelbergs, A., Van Kolen, K., Stancu, I.-C., Vasconcelos, B., Mahieu, M., Duytschaever, H., Ver Donck, L., Torremans, A., Sluydts, E., Van Acker, N., Kemp, J. A., Mercken, M., Brunden, K.R., Trojanowski, J.Q., Dewachter, I., Lee, V.M.Y., Moechars, D., 2014. Intracerebral injection of preformed synthetic tau fibrils initiates widespread tauopathy and neuronal loss in the brains of tau transgenic mice. Neurobiol. Dis. 83–95 https://doi.org/10.1016/j.nbd.2014.08.032.

Peeraer, E., Bottelbergs, A., Van Kolen, K., Stancu, I.C., Vasconcelos, B., Mahieu, M., Duytschaever, H., Ver Donck, L., Torremans, A., Sluydts, E., Van Acker, N., Kemp, J. A., Mercken, M., Brunden, K.R., Trojanowski, J.Q., Dewachter, I., Lee, V.M.Y., Moechars, D., 2015. Intracerebral injection of preformed synthetic tau fibrils initiates widespread tauopathy and neuronal loss in the brains of tau transgenic mice. Neurobiol. Dis. 73, 83–95. https://doi.org/10.1016/j.nbd.2014.08.032.

Penninkilampi, R., Casey, A.N., Singh, M.F., Brodaty, H., 2018. The association between social engagement, loneliness, and risk of dementia: a systematic review and Meta-analysis. J. Alzheimers Dis. 66, 1619–1633. https://doi.org/10.3233/JAD-180439.

Perea, J.R., García, E., Vallés-Saiz, L., Cuadros, R., Hernández, F., Bolós, M., Avila, J., 2022. p38 activation occurs mainly in microglia in the P301S Tauopathy mouse model. Sci. Rep. 12, 1–11. https://doi.org/10.1038/s41598-022-05980-8.

Peterman, J.L., White, J.D., Calcagno, A., Hagen, C., Quiring, M., Paulhus, K., Gurney, T., Eimerbrink, M.J., Curtis, M., Boehm, G.W., Chumley, M.J., 2020. Prolonged isolation stress accelerates the onset of Alzheimer's disease-related pathology in 5xFAD mice despite running wheels and environmental enrichment. Behav. Brain Res. 379, 112366. https://doi.org/10.1016/j.bbr.2019.112366.

Pietropaolo, S., Brana, C., Feldon, J., Yee, B.K., 2009. Limited impact of social isolation on Alzheimer-like symptoms in a triple transgenic mouse model. Behav. Neurosci. 123, 181–195. https://doi.org/10.1037/a0013607.

Piirainen, S., Youssef, A., Song, C., Kalueff, A.V., Landreth, G.E., Malm, T., Tian, L., 2017. Psychosocial stress on neuroinflammation and cognitive dysfunctions in Alzheimer's disease: the emerging role for microglia? Neurosci. Biobehav. Rev. 77, 148–164. https://doi.org/10.1016/j.neubiorev.2017.01.046.

Riviera-Irizarry, J.K., Skelly, M.J., Pleil, K.E., 2020 Jul 24. Social isolation stress in adolescence, but not adulthood, produces hypersocial behavior in adult male and female C57BL/6J mice. Front. Behav. Neurosci. 14, 129 https://doi.org/10.3389/fnbeh.2020.00129.

Roda, A., Serra-Mir, G., Montoliu-Gaya, L., Tiessler, L., Villegas, S., 2022. Amyloid-beta peptide and tau protein crosstalk in Alzheimer's disease. Neural Regen. Res. 17, 1666–1674. https://doi.org/10.4103/1673-5374.332127.

RStudio Team, 2020. RStudio: Integrated Development for R.

Ruan, C., Elyaman, W., 2022. A new understanding of TMEM119 as a marker of microglia. Front. Cell. Neurosci. 16, 1–4. https://doi.org/10.3389/fncel.2022.902372.

Sasaki, A., Kawarabayashi, T., Murakami, T., Matsubara, E., Ikeda, M., Hagiwara, H., Westaway, D., George-Hyslop, P.S., Shoji, M., Nakazato, Y., 2008. Microglial activation in brain lesions with tau deposits: comparison of human tauopathies and tau transgenic mice TgTauP301L. Brain Res. 1214, 159–168. https://doi.org/10.1016/j.brainres.2008.02.084.

Shen, C., Rolls, E.T., Cheng, W., Kang, J., Dong, G., Xie, C., Zhao, X.M., Sahakian, B.J., Feng, J., 2022. Associations of social isolation and loneliness with later dementia. Neurology 99, E164–E175. https://doi.org/10.1212/WNL.0000000000200583.

Sosa, L.J., Cáceres, A., Dupraz, S., Oksdath, M., Quiroga, S., Lorenzo, A., 2017. The physiological role of the amyloid precursor protein as an adhesion molecule in the developing nervous system. J. Neurochem. 143, 11–29. https://doi.org/10.1111/jnc.14122.

Sotiropoulos, I., Silva, J., Kimura, T., Rodrigues, A.J., Costa, P., Almeida, O.F.X., Sousa, N., Takashima, A., 2015. Female hippocampus vulnerability to environmental stress, a precipitating factor in tau aggregation pathology. J. Alzheimers Dis. 43, 763–774. https://doi.org/10.3233/JAD-140693.

Taylor, S.E., Morganti-Kossmann, C., Lifshitz, J., Ziebell, J.M., 2014. Rod microglia: a morphological definition. PLoS One 9. https://doi.org/10.1371/journal.pone.0097096.

Templer, V.L., Wise, T.B., Heimer-McGinn, V.R., 2019. Social housing protects against age-related working memory decline independently of physical enrichment in rats. Neurobiol. Aging 75, 117–125. https://doi.org/10.1016/j.neurobiolaging.2018.11.016.

Terwel, D., Lasrado, R., Snauwaert, J., Vandeweert, E., Van Haesendonck, C., Borghgraef, P., Van Leuven, F., 2005. Changed conformation of mutant tau-P301L underlies the moribund tauopathy, absent in progressive, nonlethal axonopathy of tau-4R/2N transgenic mice. J. Biol. Chem. 280, 3963–3973. https://doi.org/10.1074/jbc.M409876200.

Uddin, M.S., Rahman, M.M., Jakaria, M., Rahman, M.S., Hossain, M.S., Islam, A., Ahmed, M., Mathew, B., Omar, U.M., Barreto, G.E., Ashraf, G.M., 2020. Estrogen signaling in Alzheimer's disease: molecular insights and therapeutic targets for Alzheimer's dementia. Mol. Neurobiol. 57, 2654–2670. https://doi.org/10.1007/s12035-020-01911-8.

van Doeselaar, L., Yang, H., Bordes, J., Brix, L., Engelhardt, C., Tang, F., Schmidt, M.V., 2021. Chronic social defeat stress in female mice leads to sex-specific behavioral and neuroendocrine effects. Stress 24, 168–180. https://doi.org/10.1080/10253890.2020.1864319.

Vinet, J., van Weering, H.R.J., Heinrich, A., Kälin, R.E., Wegner, A., Brouwer, N., Heppner, F.L., van Rooijen, N., Boddeke, H.W.G.M., Biber, K., 2012. Neuroprotective function for ramified microglia in hippocampal excitotoxicity. J. Neuroinflammation 9, 1–15. https://doi.org/10.1186/1742-2094-9-27.

Walsh, S., Brain, J., Mukadam, N., Anderson, R., Greene, L., Govia, I., Kuhn, I., Anstey, K. J., Knapp, M., Stephan, B.C.M., Brayne, C., 2022. A systematic review of the cost-effectiveness of community and population interventions to reduce the modifiable risk factors for dementia. Maturitas 166, 104–116. https://doi.org/10.1016/j.maturitas.2022.09.002.

Wang, Y., Mandelkow, E., 2016. Tau in physiology and pathology. Nat. Rev. Neurosci. 17, 5–21. https://doi.org/10.1038/nrn.2015.1.

Wang, H., Xu, Xiaxia, Xu, Xinxin, Gao, J., Zhang, T., 2020. Enriched environment and social isolation affect cognition ability via altering excitatory and inhibitory synaptic density in mice Hippocampus. Neurochem. Res. 45, 2417–2432. https://doi.org/10.1007/s11064-020-03102-2.

Wickham, H., 2016. ggplot2: Elegant Graphics for Data Analysis.

Wright, A.L., Zinn, R., Hohensinn, B., Konen, L.M., Beynon, S.B., Tan, R.P., Clark, I.A., Abdipranoto, A., Vissel, B., 2013. Neuroinflammation and neuronal loss precede Aβ plaque deposition in the hAPP-J20 mouse model of Alzheimer's disease. PLoS One 8. https://doi.org/10.1371/journal.pone.0059586.

Würbel, H., Stauffacher, M., 1997. Age and weight at weaning affect corticosterone level and development of stereotypies in ICR-mice. Anim. Behav. 53, 891–900. https://doi.org/10.1006/anbe.1996.0424.

Zhu, D., Montagne, A., Zhao, Z., 2021. Alzheimer's pathogenic mechanisms and underlying sex difference. Cell. Mol. Life Sci. 78, 4907–4920. https://doi.org/10.1007/s00018-021-03830-w.